BIOLOGICAL CHARACTERIZATION OF CHROMATIN-TARGETED SMALL MOLECULES

Aminah Wali

A dissertation submitted to the faculty at the University of North Carolina at Chapel Hill in partial fulfillment of the requirements for the degree of Doctor of Philosophy in the Curriculum in Genetics and Molecular Biology in the School of Medicine.

Chapel Hill
2017

Approved by:

Ian Davis

Bernard Weismann

Scott Bultman

Albert Baldwin

Nate Hathaway

ABSTRACT

Aminah Wali: Biological characterization of chromatin-targeted small molecules
(Under the direction of Ian Davis)

Chromatin regulation is commonly disrupted in human cancers. The identification of chemical probes that reverse chromatin defects can provide mechanistic insights as well as therapeutic opportunities for these cancers. One such cancer is Ewing sarcoma, a pediatric bone tumor characterized by the EWSR1-FLI1 fusion protein. EWSR1-FLI1 activates an oncogenic transcriptional program by remodeling chromatin at characteristic genomic loci. To identify inhibitors of oncoprotein-mediated chromatin modulation, we adapted formaldehyde-assisted isolation of regulatory elements (FAIRE) for high-throughput use and screened a library of small molecules designed to inhibit a wide range of chromatin regulators. Among the compounds that selectively decreased chromatin accessibility at EWSR1-FLI1 binding sites, the class of histone deacetylase inhibitors was highly enriched. We found that treatment with these HDAC inhibitors altered both EWSR1-FLI1 transcript and protein levels. In addition, we identified a novel small molecule inhibitor of chromatin accessibility, UNC0621. This compound interacts directly with chromatin through nuclear protein intermediates. UNC0621 also inhibits the proliferation of Ewing sarcoma cells by inducing a cell cycle arrest. These data demonstrate the effect of chromatin-targeted small molecules on the biology of Ewing sarcoma cells, and validate the potential of chromatin-based assays to screen for compounds with therapeutic potential in cancers with epigenetic alterations.

All praises due to the Most Merciful and Benevolent Creator, who has blessed me with health, opportunities, and success.

I dedicate this work to my father (1960-2008) and mother. I have only made it this far through your love, support, and guidance. May you always be blessed.

ACKNOWLEDGEMENTS

Thank you to Dr. Ian Davis, MD, PhD for being a beyond wonderful mentor and a fantastic scientist. The help and support you have given me over the years is more than I could have asked for and your commitment to excellence has been the largest contributor to my growth as a scientist. I have no words to describe the depths of my gratitude.

I was fortunate to receive excellent guidance throughout my graduate career from my dissertation committee: Drs. Scott Bultman, Albert Baldwin, Nate Hathaway, and Bernard Weissman. Thank you all for your encouragement, scientific expertise, and support. Your input was extremely valued and undoubtedly helped me to grow as a scientist.

The greatest of thanks to the following parties: Dr. Samantha Pattenden, the Center for Integrative Chemical Biology and Drug Discovery, and Drs. Jian Jin, Kyle Butler, and Amber Mosley. This work would not have been possible without your efforts.

I also want to thank the Davis lab for the help and support over the years. I would first like to thank Andrew McFadden and Drs. Jeremy Simon, Luke Roode, and Jacob Troutman for their direct contributions to this work. And of course, I'm ever grateful for my wonderful lab mates, past and present: Mariesa Slaughter, Austin Hepperla, Tamara Vital, Shelsa Marcel, Dr. Catherine Fahey, Dr. Nick Gomez, and Dr. Dan Serber. Thank you immensely for the moral and scientific support over the years. The engaging and friendly work environment you all provided is what kept me going.

I have so many friends that provided me with great company and kept me spiritually grounded. Thank you to Dr. Cynthia Khan, Dr. Khairunnisa Yahya, Lubna Ahmed, Dr. Izna Ali, Nemah Eljabaly, Javiriyah Ashraf, Lubabatu Ahmed-Rufai, Dr. May Naji, Sana Ansari, Dr. Janan Sarwar, Nawsheen Khan, Chayla Hart, and Islem Rekik. Your friendship and sisterhood is more than I could have ever asked for.

Thank you to my siblings, Abdul-Ali Wali, Abdul-Shahid Wali, Kala Wali, Khadijah Wali, and to my mother Saida Wali (Gail Barts). You all have been my rock throughout this process and I am so grateful to you all for believing in me. Finally, thank you to my husband, Sigifredo Murrieta, for coming in at the tail end and making sure that I was rested, fed, and loved.

TABLE OF CONTENTS

LIST OF TABLES

LIST OF FIGURES

LIST OF ABBREVIATIONS

BrdU	Bromodeoxyuridine
FAIRE	Formaldehyde-assisted isolation of regulatory elements
HDAC	Histone deacetylase
PI	Propdium iodide
HT-FAIRE	High-throughput formaldehyde-assisted isolation of regulatory elements

Chapter 1: Targeting chromatin regulators in cancer

1.1: The study of epigenetics mechanisms and chromatin in disease

Epigenetics refers to changes in gene expression that does not involve changes to the underlying DNA sequence. Primarily this concerns the organization of the genome into chromatin, which consists of DNA in complex with histone proteins to form nucleosomes (1). Chromatin has varying levels of organization, with eukaryotic genomes containing regions of highly compacted chromatin as well as regions that are accessible or "open". Accessible chromatin is thought to mark regulatory regions of the genome due to occupation by factors that play key roles in the regulation of gene expression (2,3). Chromatin structure is important for compaction of DNA within the nucleus, as well as and functional domains that are crucial for cell identity and function. Consequently, disruptions in epigenetic regulatory mechanisms can result in diseases, and has shown to be involved in the development of many cancers (4).

Chromatin organization is regulated by various mechanisms and associated proteins. The first epigenetic mechanism to be thoroughly studied is DNA methylation, in which the DNA itself is methylated by modifying enzymes known as DNA methyltransferases (5). DNA methylation generally results in compaction of chromatin and is associated with gene silencing. Since the turn of the century, there has been increased study on the role of histone post-translational modifications (PTMs). The amino-terminal tails of histone proteins can undergo various forms of modification, including acetylation, methylation, and phosphorylation. These modifications are regulated by enzymes that catalyze the addition or removal of chemical groups, broadly termed "writers" and "erasers" respectively, as well as "reader" proteins that bind to

modified residues and recruit other regulatory factors (2). Together, the type of modification and the residue being modified help dictate downstream regulatory processes and research on the roles of specific histone PTMs is ongoing (6). Additionally, chromatin is also regulated by chromatin remodeling complexes, which are large and contain several protein subunits (7). Chromatin remodeling complexes possess a core subunit with ATPase activity and use energy released from ATP hydrolysis to move, exchange, or eject nucleosomes, thereby altering chromatin accessibility (8,9). Due to the widespread importance and dynamic nature of these processes, studying epigenetic mechanisms in normal development along with their perturbation in disease contexts is of great importance.

Our understanding of how epigenetic mechanisms contribute to cancer progression has been greatly increased by pairing biochemical assays with next-generation sequencing technologies. Chromatin immunoprecipitation coupled with sequencing (ChIP-seq) has permitted detection of genome-wide localization of histone post-translational modifications, which are associated with various gene regulatory functions (10,11). Additionally, the chromatin architecture of cancer genomes can be directly interrogated through the detection accessible regions of chromatin, which represent regulatory regions of the genome. Techniques such as DNase-, FAIRE- and ATAC-seq are able to isolate and map accessible regions of chromatin (3). These genome-wide chromatin-based assays, often times performed in parallel, have had great utility in determining the regulatory landscape of the genome (12).

While epigenomic approaches have proven essential to studying the chromatin state of cancer cells, they alone do not provide the full picture of the mechanisms at play. To better understand the cause of chromatin alterations, they can be studied in the context of other molecular aberrations that occur in cancer. Modern genomics approaches have allowed for broad

mutational analysis of cancer genomes and have shown epigenetic regulators to be highly mutated(13–15). Moreover, certain cancers primarily select for chromatin-modulating aberrations. For example, clear cell renal cell carcinoma frequently harbors loss or mutation of chromatin regulators(16), and loss of a chromatin remodeler is found in nearly all malignant rhabdoid tumors (7,17).

1.2: Chromatin regulators as therapeutic targets

Whereas alterations at the DNA sequence level are considered static, epigenetic mechanisms are dynamic and changes in chromatin can persist over cell divisions. Understandably, chromatin-modulating proteins have emerged as attractive potential therapeutic targets in various cancers (18,19). In recent decades, epigenetically-targeted compounds have become widely used in both research and the clinic, with some even becoming FDA-approved therapies (20). The first of these was 5'-azacytidine, a DNA methyltransferase inhibitor that was approved for patients with myelodysplastic syndrome (21,22). Histone deacetylase (HDAC) inhibitors have also seen success in the clinic. Two HDAC inhibitors, Vorinostat and Romidepsin, have been approved by the FDA for certain hematological malignancies (23). Panbinostat, another HDAC inhibitor, was approved in 2015 for the treatment of multiple myeloma (24). Dozens of other chromatin-targeted small molecules are currently used in research and clinical trials, and still many more are being developed (20,25–27).

Although inhibitors for DNA methyltransferases and histone deacetylases have seen success, these compounds are also notorious for their pleiotropic effects and lack of clear mechanism of their effect on cancer biology (28). Movement towards targeted therapeutic approaches has lead to development and application of epigenetic inhibitors based on importance

of a target in a particular cancer. EZH2, a methyltransferase and component of the Polycomb repressive complex 2 (PRC2), has emerged as an attractive target as gain-of-function mutations or overexpression of EZH2 is a feature of several cancers (29). EZH2 inhibitors (EZH2i) are currently being utilized to study its role in these cancers, as well as to explore potential therapeutic benefit of targeting EZH2 (4,30).

While significant focus has been on enzymes that modify histones, there is an increasing interest in non-enzyme chromatin regulators as potential targets (25). This includes reader proteins, which recognize and bind to histone post-translational modifications, thereby controlling downstream gene regulatory processes (31). Belonging to this protein class is the BET family of readers, which bind to acetyl-lysine residues on histones. BRD4, a member of this family, is involved in a recurrent fusion in a rare pediatric carcinoma, leading to the BRD4-NUT oncoprotein (32). In an effort to target this fusion protein, the compound JQ1 was developed as an inhibitor of BRD4 and was the first of the BET inhibitors (BETi). In addition to being widely utilized in research to study the role of BET proteins in cellular processes and cancer models, BETi exhibit therapeutic potential and are currently in phase I clinical trials for various indications (33–35). The success of BETi and EZH2i represent examples of how development of new chromatin-targeted small molecules and identification of new targets is paving way for future cancer treatments.

1.3: Targeting EWSR1-FLI1 in Ewing Sarcoma

One cancer of interest is Ewing sarcoma, a bone and soft tissue sarcoma affecting children and young adults for which there are currently no approved targeted therapies (36). Interestingly, the cancer is characterized by a genetic aberration that occurs in upwards of 85%

of cases: a translocation between chromosomes 11 and 22 that fuses the N-terminal portion of EWSR1 to the C-terminal portion of FLI1, generating the EWSR1-FLI1 chimera (37). FLI1 is an ETS transcription factor, and the DNA binding domain of FLI1 is retained in EWSR1-FLI1. In the context of the fusion protein, the N-terminal domain of EWSR1 functions as a transactivation domain, allowing EWSR1-FLI1 to activate an aberrant transcriptional network (38,39). It has also been shown that EWSR1-FLI1 activity is necessary for continued growth of Ewing sarcoma cells (40,41). Therefore, EWSR1-FLI1 functions as an oncogenic transcription factor and a primary driver of Ewing sarcoma.

To better understand the oncogenic activity of EWSR1-FLI1, a previous study from our research group analyzed genomic differences in cells expressing either the parental transcription factor FLI1 or the fusion protein. We observed by ChIP-seq that, in spite of retaining the DNA binding domain of FLI1, EWSR1-FLI1 exhibited divergent binding across the genome (42). To analyze the chromatin organization at EWSR1-FLI1-bound regions, we utilized Formaldehyde-assisted Isolation of Regulatory Elements (FAIRE), a biochemical assay that selectively isolates regions of accessible chromatin. We observed that regions bound by EWSR1-FLI1 in Ewing sarcoma cells were characteristically marked by high FAIRE signal, indicating highly accessible chromatin. Moreover, upon silencing the fusion gene in Ewing sarcoma cells by RNAi, FAIRE signal at EWSR1-FLI1-bound regions decreased. This indicated that EWSR1-FLI1 was necessary for maintaining accessible chromatin at its binding sites. Additionally, since many of these sites are near EWSR1-FLI1 target genes that are known to contribute to cellular transformation, these data suggested that the ability of EWSR1-FLI1 to maintain open chromatin is necessary for its oncogenic activity.

The pattern of accessibility at oncoprotein-bound sites provided evidence for a unique chromatin signature in Ewing sarcoma (42). However, the cause of this phenotype was not apparent based on the known functions of the parental proteins. FLI1 belongs to the ETS family of transcription factors, and EWSR1 is an RNA binding protein that has also been shown to be involved in transcription (43,44). Since neither protein is a known chromatin modifier, the mechanism driving increased EWSR1-FLI1-dependent chromatin accessibility in Ewing sarcoma remained unclear.

Due to the presence of the fusion in the vast majority of Ewing sarcoma cases and its importance for the biology of the cancer, EWSR1-FLI1 is an attractive potential therapeutic target. However, there are gaps in our knowledge of how this protein functions in the cancer, and EWSR1-FLI1 is technically challenging to study in a biologically relevant context (45). Additionally, because EWSR1-FLI1 is a transcription factor and does not possess "druggable" catalytic domains, there are limited options for targeting the fusion protein directly. Rather, dependencies and interactions of the oncoprotein present a more promising avenue for mechanistic and therapeutic targeting. The chromatin signature we observed in Ewing sarcoma cells indicated a potential dependency on epigenetic regulators for EWSR1-FLI1 activity, which we hypothesized could be exploited to inhibit oncogene activity. This report describes our approach to determine mechanisms important for EWSR1-FLI1-mediated chromatin modulation, and my studies on the biological function of compounds that alter chromatin accessibility in Ewing sarcoma.

Chapter 2: A high-throughput small molecule screen identifies inhibitors of aberrant chromatin accessibility[1]

2.1: Introduction

A growing range of human cancers has been associated with mutations in genes encoding proteins that regulate affect chromatin, the assembly of proteins and DNA that regulates DNA-templated processes including transcription and replication (15,46). Small molecule drugs and chemical probes offer an approach to explore the biological consequences of these mutations and are emerging as a therapeutic strategy to target disease pathways. Drugs targeting histone deacetylase enzymes (HDAC), the bromodomain reader BRD4, and DNA methylation have already received regulatory approval or have entered clinical testing, and chemical probes have been developed against a broad range of chromatin regulators such as the methyltransferases (47) DOT1L (48), EZH2 (30,49,50), and G9a (51,52), and the reader proteins L3MBTL3 (53), and BRD4 (32,54). Transcription factors that lack enzymatic activity or binding pockets with targetable molecular features have been considered "undruggable", and a reductionist approach based on identification of their molecular targets has largely failed.

The majority of Ewing sarcoma, a highly malignant pediatric bone and soft tissue tumor, harbors the chromosomal translocation t(11;22)(q24;q12), which joins the amino terminal

---

[1] This work was previously published in the Proceedings of the National Academy of the Sciences. Pattenden SG, Simon JM, Wali A, Jayakody CN, Troutman J, McFadden AW, Wooten J, Wood CW, Frye SV, Janzen WP, Davis IJ. High-throughput small molecule screen identifies inhibitors of aberrant chromatin accessibility. Proc Natl Acad Sci. 2016 Feb 29;201521827. Available from: http://www.pnas.org/lookup/doi/10.1073/pnas.1521827113

domain of *EWSR1* with the DNA binding domain of the ETS transcription factor family member *FLI1* to generate the chimeric transcription factor EWSR1-FLI1 (55). Translocations with other ETS genes are detected in most of the remaining tumors yielding similarly functioning fusion proteins (37). We recently found that, despite conservation of the ETS DNA binding domain, the fusion oncoprotein uniquely localizes to specific microsatellite regions (42,56). Using formaldehyde-assisted isolation of regulatory elements (FAIRE), a biochemical strategy to enrich for nucleosome depleted regions of chromatin, we demonstrated that EWSR1-FLI1 binding was necessary to maintain nucleosome depletion at these sites. The mechanism through which EWSR1-FLI1 modifies chromatin remains unknown. EWSR1-FLI1 does not possess recognizable catalytic activity, so other yet-to-be-identified proteins likely mediate its ability to remodel chromatin.

The absence of a biochemical mechanism would typically pose challenges for chemical targeting. However, we hypothesized that reversing a unique chromatin signature could serve as a strategy to discover small molecules with activity toward EWSR1-FLI1. To target this activity, we adapted and validated FAIRE as an automated, high-throughput tool and applied this method to evaluate a focused set of small molecules designed to interact with proteins that regulate chromatin. Because this approach directly assessed the effects of compounds on a specific, disease-associated aberrant chromatin signature, while remaining agnostic about precise molecular mechanisms, it enabled the discovery of agents that affect the underlying molecular defect without requiring an *a priori* selection of molecular targets.

2.2: Validation of column-based FAIRE

As currently applied, FAIRE, a biochemical assay for the enrichment of nucleosome-

depleted regions of the genome, is dependent on organic extraction with a mixture of phenol and chloroform. Since this critical extraction step is not easily automated, we adapted and miniaturized FAIRE by substituting organic extraction with solid-phase selection and robotic automation, hereafter termed high throughput FAIRE (HT-FAIRE) (Fig. 2.1A). Since the chromatin fractionation step is central to this technique, we compared the performance of these methods. Quantitative locus-specific testing demonstrated that both approaches offered concordant enrichment at a series of promoter and enhancer regions (Fig. 2.2). We then compared the performance of both methods genome-wide. For these studies we used primary human endothelial cells (HUVEC) since multiple genomic datasets exploring chromatin features have been generated for these cells permitting subsequent integrative analyses of the FAIRE results (ENCODE Tier 2, (12)).HT-FAIRE signal mimicked that of standard FAIRE. Enrichment at active transcriptional start sites (TSS) positively correlated with RNA abundance, as well as enrichment at CTCF sites, consistent with previously described FAIRE studies (Fig. 2.1B-D) (57). Signal enrichment by HT-FAIRE was less robust at TSS, consistent with the qPCR results. Of the top 10,000 nucleosome-depleted regions detected in HUVEC by HT-FAIRE, approximately 90% overlapped those sites identified by standard FAIRE. In contrast, fewer than 50% of enriched regions overlapped FAIRE sites from any of six other cell lines (Fig. 2.3A), demonstrating that HT-FAIRE offers a level of specificity similar to that reported in previous studies that compared standard FAIRE between cell types (58).

We then specifically examined those genomic regions that most discriminate HT- and standard FAIRE and also demonstrate HUVEC cell-type specificity. Hierarchical clustering of these ~9,700 genomic regions identified three groups. Cluster 1 (1,805 regions) consisted of those regions with FAIRE enrichment in all cell lines examined by standard FAIRE but lacked

signal in HT-FAIRE. Cluster 2 (6,017 regions), by far the largest, consisted of regions with HUVEC-specific signal enrichment that was detected by both HT- and standard FAIRE. Cluster 3 (843 regions) consisted of regions selectively identified by HT-FAIRE (Fig. 2.1F). Regions in each cluster were then associated with genes (Genome Regions Enrichment of Annotations Tool (GREAT), (59)).

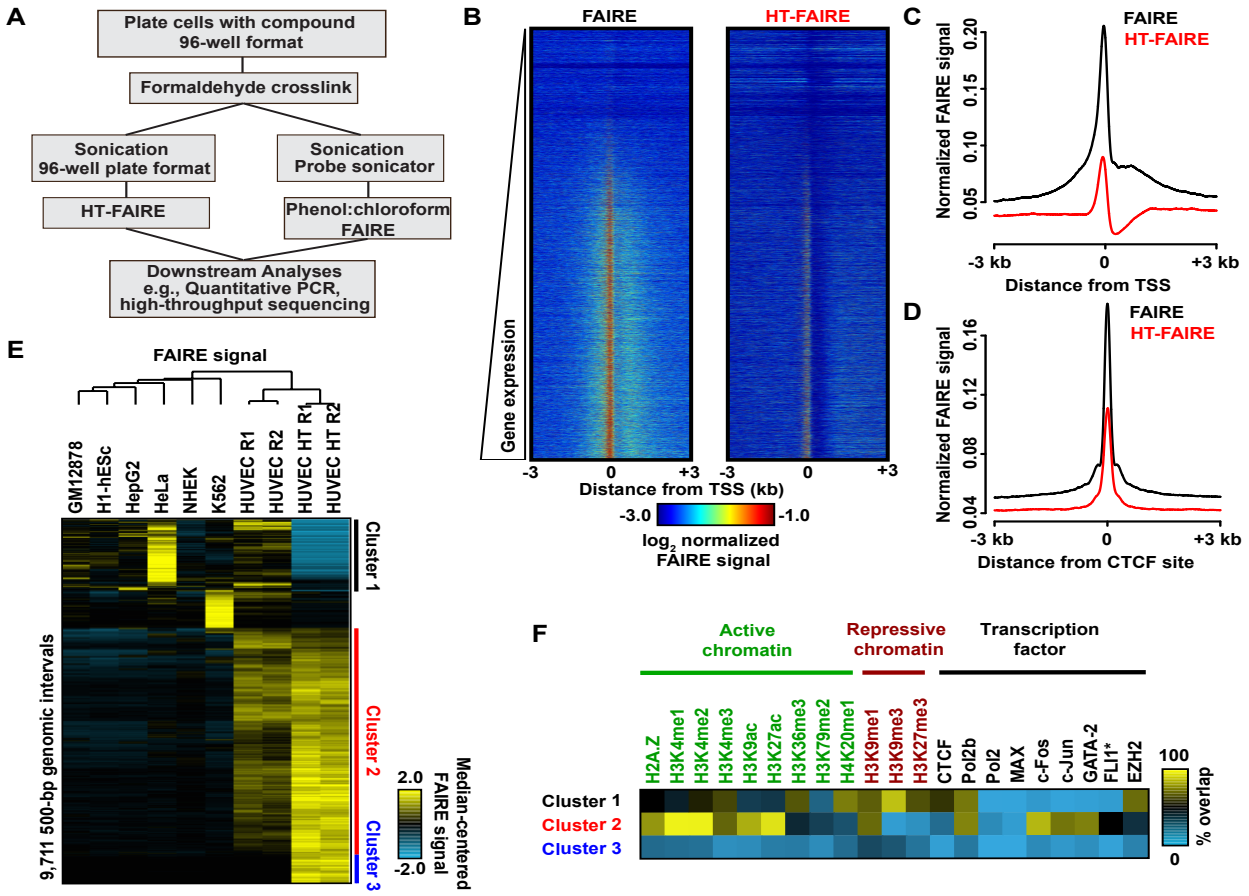

Figure 2.1: Comparison of FAIRE methodologies. **(A)** Flow diagram comparing column-based and standard FAIRE methods. **(B)** Heatmap representation of normalized FAIRE enrichment (± 3 kb from TSS) using standard (left) or column (right) FAIRE in HUVEC. **(C)** Normalized FAIRE signal from both methods ± 3 kb from TSS. **(D)** Normalized FAIRE signal from both methods ± 3 kb around HUVEC CTCF sites (ENCODE). **(E)** Fraction of top 10,000 HT-FAIRE enriched sites overlapping standard FAIRE sites from HUVEC and 6 other cell types (ENCODE). **(F)** Hierarchical clustering analysis of 500 bp intervals demonstrating differential FAIRE signal across 7 cell types as well as HUVEC HT-FAIRE. Platform-specific (Clusters 1 and 3) and cell-type-specific (Cluster 2) clusters were identified.

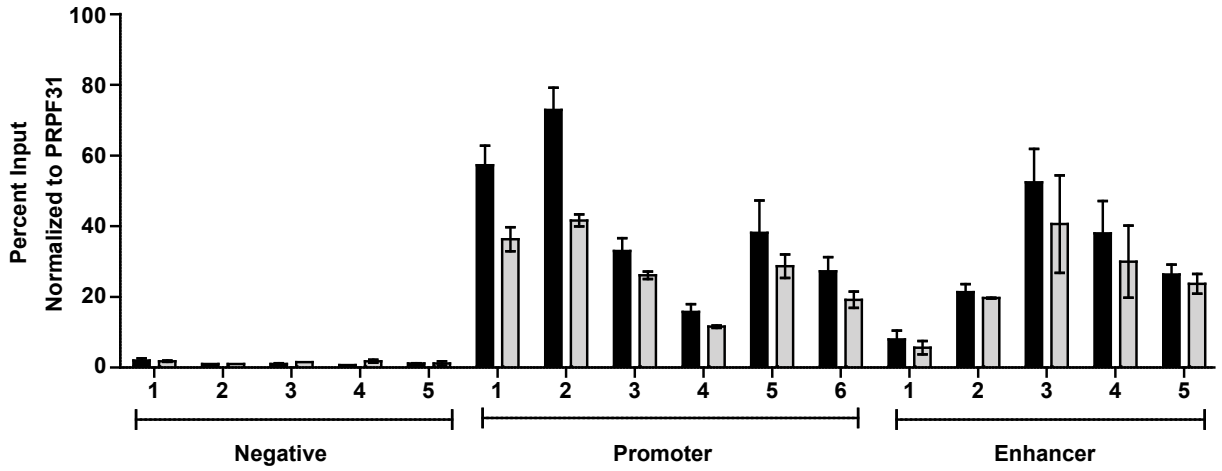

Figure 2.2: Comparison of standard versus HT-FAIRE by quantitative PCR (qPCR). Chromatin was prepared from endothelial (HUVEC) cells and divided in half, and input was reserved. Each half was subjected to standard (black bars) or column-based (gray bars) FAIRE followed by qPCR. Primer sets included regions that are negative (Negative) for FAIRE signal, promoter regions (Promoter) from actively transcribed genes, and enhancer regions (Enhancer) (Table 2.3). Percent input (ΔCt) values were normalized to a genomic region near the PRPF31 gene that is negative for FAIRE signal. Error bars represent the SE of two biological replicates with two technical replicates each.

As expected, the HUVEC-selective sites detected by both HT- and standard FAIRE (Cluster 2) were tightly linked with endothelial cell ontologies including angiogenesis ($q = 4.4 \times 10^{-12}$) and regulation of cell-substrate adhesion ($q = 6.5 \times 10^{-7}$) (Fig. 2.3B). No significant gene ontologies were associated with the regions in the other clusters. To test whether FAIRE-enriched regions were likely to harbor regulatory elements, we annotated the sites from each cluster with active (H2A.Z, H3K4me1, H3K4me2, H3K4me3, H3K9ac, H3K27ac, H3K36me3, H3K79me2, H4K20me1) and repressive histone modifications (H3K9me1, H3K9me3, H3K27me3). We also tested association with numerous transcription factors that are known to be important in endothelial cell biology (CTCF, RNA Polymerase II, MAX, FOS, JUN, GATA2, FLI1, EZH2) as assessed by ChIP-seq (12,42) (Fig 2.1F). Sites in Cluster 2 (common to both

platforms, HUVEC-specific) were associated primarily with active histone modifications as well as sites targeted by FLI1, FOS, JUN, GATA2, and RNA Polymerase II.

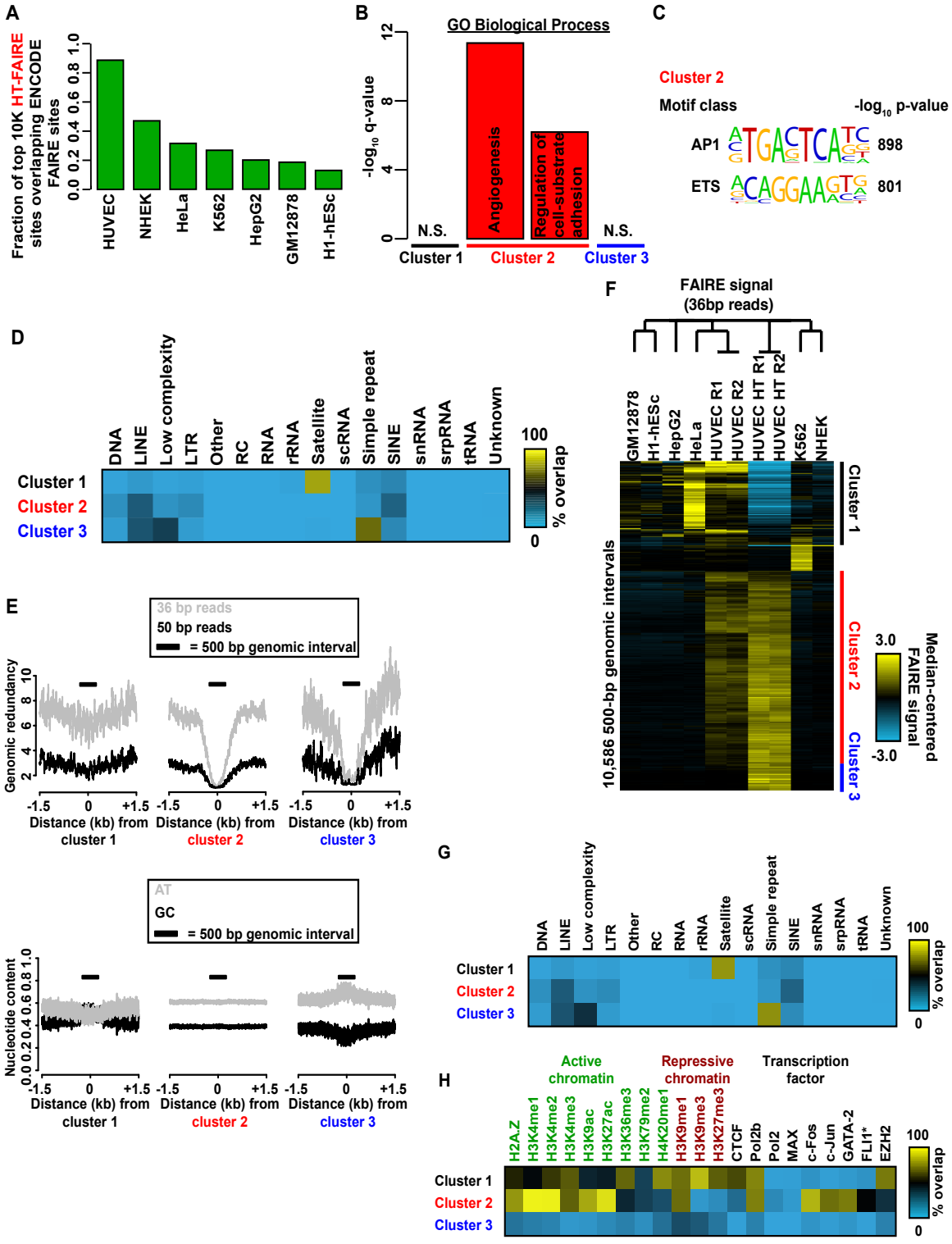

Figure 2.3: Comparison of FAIRE methodologies. (A) Fraction of top 10,000 HT-FAIRE enriched sites overlapping standard FAIRE sites from HUVEC and six other cell types (ENCODE). **(B)** Ontology enrichment (GREAT) of genes associated with sites in clusters 1–3 (Fig. 2.1E)**(C)** Highly enriched TF motifs in cluster 2. Clusters 1 and 3 did not have any motifs determined to be significant by a multicomponent test (*Methods*). **(D)** Mappability (*Left*) and nucleotide content (*Right*) within 1.5 kb of sites from clusters 1–3 (Fig. 2.1E). Mappability was assessed for both 36- and 50-bp reads. Genomic redundancy refers to the number of times a given 36- or 50-mer occurs in the reference genome. 500 bp window indicated by bar. **(E)** Fractional overlap annotation of clusters 1–3 (Fig. 2.1E) with repetitive element classes. **(F)** Fractional overlap annotation of clusters 1–3 (H) with histone modifications and transcription factor ChIP-seq peak calls (ENCODE). **(G)** Fractional overlap annotation of clusters 1–3 (H) with repetitive element classes (RepeatMasker). **(H)** Hierarchical clustering analysis of ENCODE FAIRE signal in 500-bp intervals from seven cell types, as well as HUVEC HT-FAIRE after truncation of 50-bp reads to 36 bp. Identified clusters exhibit method specificity (clusters 1 and 3) and cell-type specificity (cluster 2).

The prevalence of putative FLI1 and FOS/JUN binding sites was corroborated by the enrichment of ETS and AP1 DNA sequence motifs in these regions ($p < 1 \times 10^{-800}$, Fig. 2.3C). ETS (specifically ETV2) and AP1 factors are both known to play prominent roles in endothelial development (60,61). Regions in cluster 1 were more closely associated with repressive modifications and EZH2 binding (Fig 2.1F). Clusters 1 and 3 were distinguished by enrichment for repetitive regions, with each cluster associated with a specific repetitive element class: satellites (82% of Cluster 1 sites) and simple repeats (71% of Cluster 3 sites) (Fig. 2.3D). We also noted a difference in sequence composition between Cluster 1 and Clusters 2 and 3 (Fig. 2.3E). The basis of their differential enrichment may reflect chromatin variation at these regions that are distinguished by the biochemical properties specific to organic or solid phase purification. Because we used published standard FAIRE datasets that were generated with a shorter sequencing read length (ENCODE, 36-bp reads), we asked whether the difference in read length could partially account for the variability in mapping and sequence content at Clusters 1 and 3 (Fig. 2.3F). Repeating these analyses after truncating the HT-FAIRE sequencing reads to

36 bp did not change the hierarchical clustering or histone modification associations (Fig. 2.3 G and H). Taken together these data demonstrate that HT-FAIRE performs similarly to standard FAIRE and identifies regions that are biologically meaningful.

2.3: Application of HT-FAIRE to small molecule screening

After validating solid phase purification we adapted the method for high throughput automation and applied it in a targeted screen. The screen was based on two regions (P1 and P7) that were selected from a set of Ewing sarcoma-specific sites a region that we had previously shown was were aberrantly accessible in multiple Ewing sarcoma cell lines with accessibility that was dependent on continued expression of EWSR1-FLI1 (42). Two control regions that consistently demonstrate FAIRE enrichment (AURKAIP1) or lack of enrichment (BC006361) across many cell types were also tested. We performed the screen using a custom library that consisted of 640 small molecules, including those designed to target histone methyltransferases, methyl lysine reader proteins, histone demethylases and deacetylases, DNA methyltransferases, and acetyl-lysine reader proteins. A Ewing sarcoma patient-derived cell line that grows in suspension culture (EWS894) was first tested for DMSO tolerance (Fig. 2.4). The unit automation pipeline separated each of two 384-well compound plates containing the library into four 96-well plates for screening (Fig. 2.5). Cells were then exposed to 10 μM of each compound (or DMSO control) for 16 hours. Following HT-FAIRE, samples from the 96-well plates were combined into a 384-well plate format for qPCR-based testing of the signature and control regions in two technical replicates. The positive control region demonstrated a statistically significant difference in FAIRE signal over the background control (Plate 1, $p = 7.50e-53$; Plate 2, $p = 6.63e-98$). Critically, signal from each of the disease-specific regions were highly

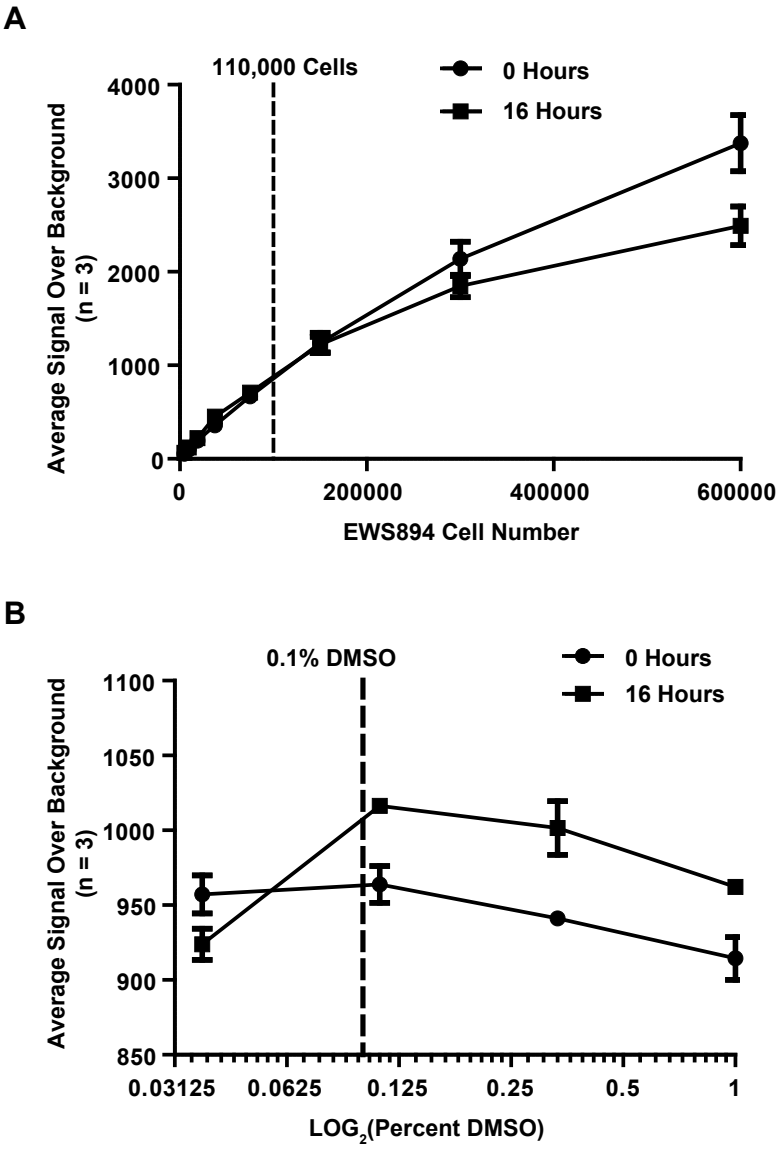

Figure 2.4: EWS894 cell number and DMSO tolerance for HT-FAIRE assay. (*A*) Assay showing cell viability at increasing cell density in a 96-well plate after 16-h incubation. A plating density of 1.1×10^5 cells per well was selected for the assay (dotted line). The *x* axis shows cell number. The *y* axis shows the average luminescent signal over background (media only). Error bars represent the SD of three replicates. (*B*) Assay showing cell viability after 16-h treatment of 1.1×10^5 EWS894 cells per well with twofold dilutions of DMSO ranging from 1% to 0.03125%. Cells begin to lose viability at DMSO concentrations higher than 0.1% (dotted line). The *x* axis shows the LOG_2-transformed percent DMSO concentration. The *y* axis shows the average luminescent signal over background (no DMSO). Error bars represent the SD of three replicates.

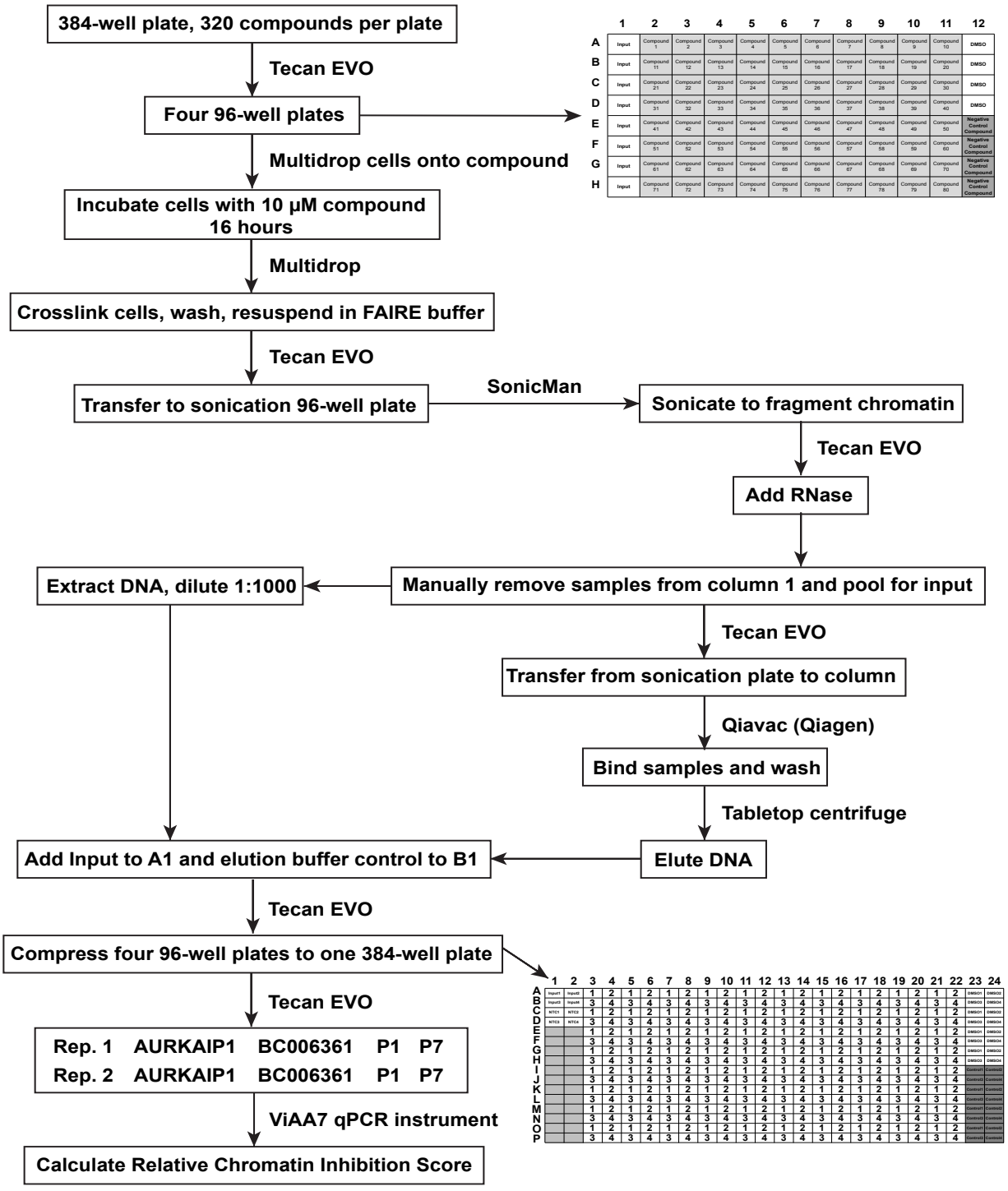

Figure 2.5: Flowchart outlining the automation steps for HT-FAIRE.

concordant (Pearson r = 0.8764), which supported combining the values from both sites for subsequent analytics (Fig. 2.6*A*).

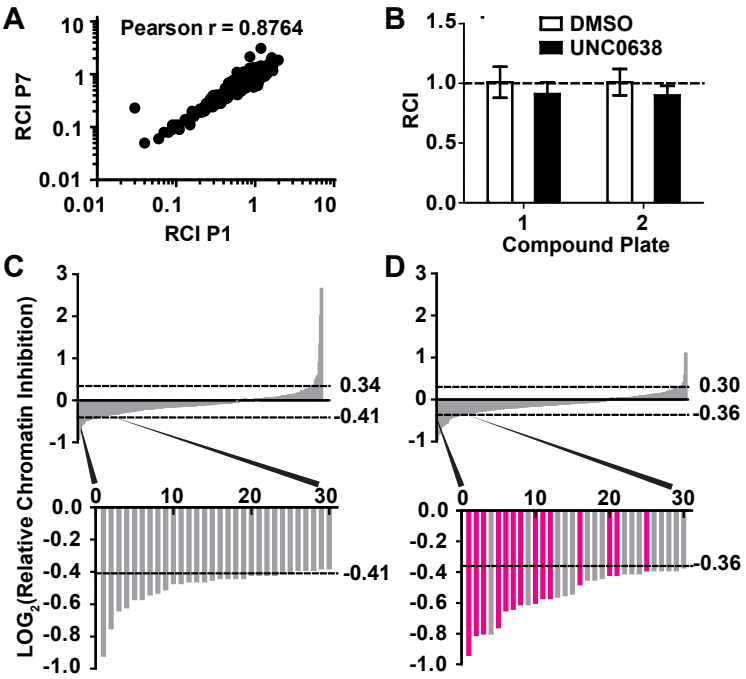

Figure 2.6: Chromatin signature-based screen identified a cluster of HDAC inhibitors that significantly decreased EWSR1-FLI1-dependent chromatin accessibility. **(A)** The LOG_{10} transformed relative chromatin inhibition (RCI) scores for the Ewing sarcoma specific P1 and P7 regions are plotted. Since they showed a strong correlation (Pearson r = 0.8764) these values were averaged for the final RCI score. **(B)** RCI scores for DMSO and a negative control compound, UNC0638 are plotted for each 384-well plate. An RCI score of 1.0 indicates no change (dotted line). Error bars are the standard deviation of 16 replicate samples. **(C-D)** The chromatin-focused library consists of two 384-well compound plates (640 compounds total). Plate 1 **(C)** or Plate 2 **(D)** LOG_2 ratio of the relative chromatin inhibition values was plotted against the rank order of compounds from greatest relative decrease (top, left side of X-axis) to the greatest relative increase (top, right side of X-axis) in FAIRE signal following compound treatment. The dashed lines indicate the significance cutoff of relative chromatin inhibition values greater or less than two standard deviations from the average RCI for vehicle-treated controls. Thirty compounds that show the greatest decrease in FAIRE signal for each plate are magnified (bottom graph). The bars representing HDAC inhibitors are highlighted in magenta.

To quantify the degree to which chromatin accessibility changed following compound treatment, we calculated a "relative chromatin inhibition" (RCI) score that compared the relative

enrichment at the oncogene-targeted regions to that at the positive control region. Compounds that affected both the oncogene-targeted and controls regions were considered non-specific. A RCI score of 1.0 was considered "no change". Replicates of controls DMSO (vehicle) and UNC0638 (26) (a chemical probe that we had previously determined not to affect aberrantly open chromatin in Ewing sarcoma cells) demonstrated an RCI of 1.0 (Figs. 2.6B and S5A). Since this primary screen was based on a single measurement, we permitted greater intersample variability, defining compounds with an RCI value greater than two SDs from the mean RCI score for DMSO-treated controls as "hits" (Figs. 2.6B and S5A) (62). Fifty-eight compounds met criteria for reduced chromatin accessibility (Fig. 2.6C-D). Forty-three of these compounds were uncharacterized, 14 of which were analogs within a single chemical scaffold, and 15 were characterized chemical probes. Treatment with 20 compounds resulted in increased FAIRE signals, all of which were uncharacterized (Table 2.1). Because the goal of this study was to inhibit EWSR1-FLI1-mediated aberrant chromatin accessibility, we focused on those compounds that decreased the FAIRE signal.

We then prepared a secondary screen plate that contained these compounds and 16 compounds that failed to show a change in chromatin accessibility in the initial screen (RCI of 1.0, no change). This secondary screen was performed on three independent replicates of EWS894 cells, permitting us a more stringent threshold of 3 SDs from the mean RCI score to define hits (62,63) Fifteen compounds (26%) met this enhanced threshold (Fig 2.8A and S5B).

Remarkably, of the 21 HDAC inhibitors that were included in our library, 14 of these compounds scored as hits in both the primary and secondary screens (Fig. 2.8A). We compared the specificity of the active and inactive HDAC inhibitors (Table 2.2). Although the majority of the inhibitors in our set have known activity against multiple HDAC proteins making it difficult

A

	Relative Chromatin Inhibition		
Plate	**Average DMSO Value**	**Standard Deviation**	**Cutoff for 2 SD**
1	1.01	0.13	0.75
2	1.01	0.11	0.78

B

	Relative Chromatin Inhibition		
Plate	**Average DMSO Value**	**Standard Deviation**	**Cutoff for 3 SD**
Hits	1.00	0.03	0.91

Figure 2.7: Cutoff values for HT-FAIRE screen hits. (*A*) Compounds were assigned as a hit for the HT-FAIRE screen if they had an RCI score of ≤2 SDs from the average DMSO RCI score. (*B*) Compounds were assigned as a hit in the HT-FAIRE secondary screen if they had an RCI score of ≤3 SDs form the average DMSO RCI score.

Plate	FAIRE Signal	Target Category	Chemical Category	Number of Hit Compounds
1	Decrease	methyl lysine reader	uncharacterized	8
		DNA methyltransferase	chemical probe	1
		lysine methyltransferase	uncharacterized	16
	Increase	methyl lysine reader	uncharacterized	6
		lysine methyltransferase	uncharacterized	6
2	Decrease	histone deacetylase	chemical probe (Table S2)	14
		methyl lysine reader	uncharacterized	10
		lysine methyltransferase	uncharacterized	6
		arginine methyltransferase	uncharacterized	3
	Increase	methyl lysine reader	uncharacterized	5
		lysine methyltransferase	uncharacterized	3

Table 2.1: Compounds that produced a statistically significant change in FAIRE signal

to identify the specific HDAC target, inhibitors selective for HDAC6 (Tubastatin) (64) and HDAC8 (PCI-34051) (65) did not score in our screen, making it unlikely that either of these HDAC proteins are involved in maintaining aberrant chromatin accessibility in Ewing sarcoma. The overall reproducibility of the screen and in particular for HDAC inhibitors in the secondary screen confirms the robustness of HT-FAIRE as an approach for discovering biologically relevant compounds using a small, focused compound library. *A priori* selection of inhibitors of HDAC proteins as lead candidates for screening would have been unlikely since histone hyperacetylation is commonly associated with destabilized nucleosomes and open chromatin. To replicate the results of the screen, we focused on 2 hit compounds, Vorinostat and Panobinostat, since these hydroxamate derivatives inhibit multiple classes of HDACs and have received FDA approval for oncological indications (66). Treatment of EWS894 cells for 16 hours with either of these compounds followed by HT-FAIRE resulted in a dose-dependent decrease in chromatin accessibility (Fig. 2.8A). This decrease was not observed with an HDAC inhibitor that did not score as a hit in our screen (Tubastatin), or a compound with an unrelated structure and protein target.

We then validated the compounds that emerged from our screen using standard FAIRE-qPCR. FAIRE signal from cells treated for 16 hours with Panobinostat decreased at the test regions to a similar extent (~2-fold) to that observed in the screen, and also demonstrated a similar effect on two additional EWSR1-FLI1-targeted sites (Fig. 2.8B). Critically, positive control regions remained unaffected, demonstrating that the decreased RCI was not the result of increased signal at the control regions. We then validated the effect of additional HDAC inhibitors by standard FAIRE. Panobinostat, Vorinostat and AR-42 demonstrated a similar magnitude effect on chromatin (Fig. 2.8C). Panobinostat also led to a dose-dependent decrease in

HDAC inhibitor	Hit?	HDAC Target	References
Panobinostat (LBH-589)	Yes	HDAC1, HDAC2, HDAC3, HDAC6	Blood. 2005 Feb 15;105(4):1768-76.
AR-42 (HDAC-42)	Yes	Pan inhibitor	J Med Chem. 2005 Aug 25;48(17):5530-5.
Trichostatin A (TSA)	Yes	Pan inhibitor	J Biol Chem. 1990 Oct 5;265(28):17174-9.
Vorinostat (SAHA)	Yes	HDAC1, HDAC2, HDAC3, HDAC6	Proc Natl Acad Sci U S A. 1998 Mar 17;95(6):3003-7.
Entinostat (MS-275)	Yes	HDAC1, HDAC2, HDAC3, HDAC9	Proc Natl Acad Sci U S A. 1999 Apr 13;96(8):4592-7.
Abexinostat (PCI-24781)	Yes	HDAC1, HDAC2, HDAC3, HDAC6, HDAC10	Mol Cancer Ther. 2006 May;5(5):1309-17.
Dacinostat (NVP-LAQ824)	Yes	HDAC1, HDAC3, HDAC4, HDAC6	Blood. 2003 Oct 1;102(7):2615-22. Epub 2003 Jun 19; Cancer Res. 2004 Jan 15;64(2):689-95.
Quisinostat (JNJ-26481585)	Yes	Pan inhibitor	Leukemia. 2009 Oct;23(10):1894-903.
CUDC-101	Yes	Pan-HDAC, EGFR, HER2	J Med Chem. 2010 Mar 11;53(5):2000-9.
Pracinostat (SB939)	Yes	Pan inhibitor	Mol Cancer Ther. 2010 Mar;9(3):642-52.
Givinostat (ITF2357)	Yes	HDAC1, HDAC2, HDAC3, HDAC4, HDAC6, HDAC7	J Hepatol. 2005 Feb;42(2):210-7.
CUDC-907	Yes	Pan-HDAC and PI3K	Clin Cancer Res. 2012 Aug 1;18(15):4104-13
M344	Yes	Pan inhibitor	J. Med. Chem., 1999, 42 (22), pp 4669–4679
Romidepsin (FK228)	Yes	HDAC1, HDAC2, HDAC3, HDAC8	J Antibiot (Tokyo). 1994 Mar;47(3):301-10.
Tubastatin HCl	No (Negative Control)	HDAC6	J Am Chem Soc. 2010 Aug 11;132(31):10842-6
Belinostat (PXD101)	No	HDAC1, HDAC2, HDAC3, HDAC6	Mol Cancer Ther. 2003 Aug;2(8):721-8.
Mocetinostat (MGCD0103)	No	HDAC1, HDAC2	Mol Cancer Ther. 2008 Apr;7(4):759-68
Droxinostat	No	HDAC3, HDAC6, HDAC8	Mol Cancer Ther. 2010 Jan;9(1):246-56.
MC1568	No	HDAC4, HDAC5, HDAC7, HDAC9	J Med Chem. 2005 May 5;48(9):3344-53.
PCI-34051	No	HDAC8	Leukemia. 2008 May;22(5):1026-34.
Tacedinaline (CI-994)	No	HDAC1, HDAC2, HDAC3	Cancer Res. 1993 Jul 1;53(13):3008-14; Mol Cancer Ther. 2003 Apr;2(4):401-8.

Table 2.2: Histone deacetylase inhibitors included in the compound library. Histone deacetylase inhibitors, specification of screening status, and recognized HDAC target specificity are shown.

FAIRE signal at an EWSR1-FLI1 targeted site (Fig. 2.8D). As further validation, we performed FAIRE-qPCR in two additional patient-derived EWSR1-FLI1-expressing Ewing Sarcoma cell

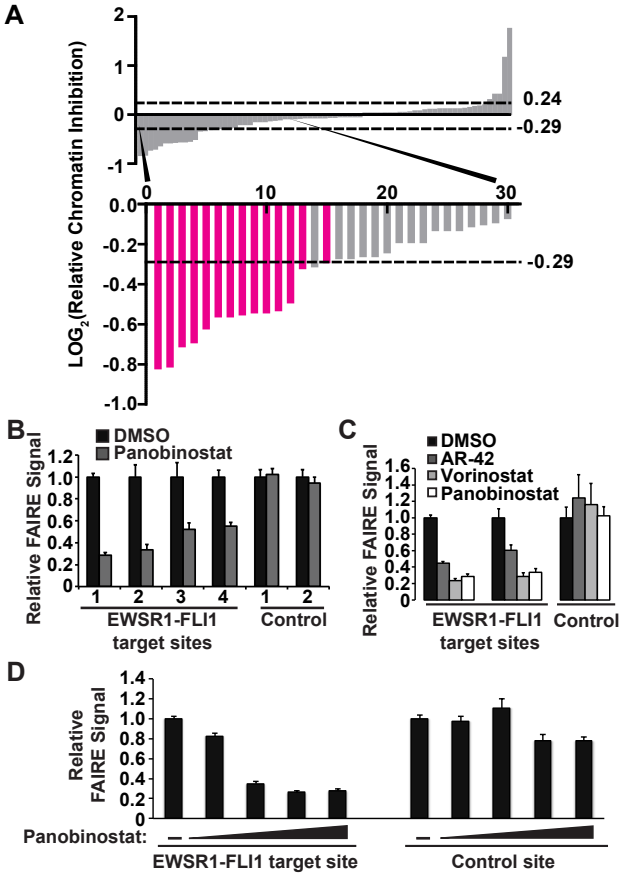

Figure 2.8: HDAC inhibitors affect EWSR1-FLI1 chromatin accessibility in a dose-dependent manner. **(A)** Secondary screen that included all hit compounds from Plate 1 and Plate 2 and a selection of compounds that did not score. LOG_2 ratio of the RCI values as described for Fig. 2*C-D*. The dashed lines indicate the significance cutoff of RCI values greater or less than three standard deviations from the average RCI for vehicle-treated controls. The bars representing HDAC inhibitors are highlighted in magenta. **(B)** Standard FAIRE-qPCR was performed on EWS894 cells treated with Panobinostat for EWSR1-FLI1 target sites and control sites (**C**) Standard FAIRE-qPCR was performed on EWS894 cells treated with Vorinostat, AR-42, or Panobinostat. (**D**) FAIRE-qPCR was performed on an EWSR1-FLI1 binding site (P1) and a control site (AURKAIP1) after treatment of EWS894 cells with DMSO or 10-fold dilutions of Panobinostat (10 μM to 0.01 μM). All treatments were 10 μM for 16 h unless otherwise noted. FAIRE is plotted relative to DMSO control, and error bars represent the SD of three replicates.

lines, EWS502 (Fig. 2.8B) and RD-ES (Fig. 2.8C). Panobinostat treatment for 16 hours significantly decreased FAIRE signal at EWSR1-FLI1 binding sites in both of these cell lines. Together, these data confirm that HDAC inhibitors are associated with reduced chromatin accessibility at EWSR1-FLI1-targeted regions as measured by both HT- and standard FAIRE.

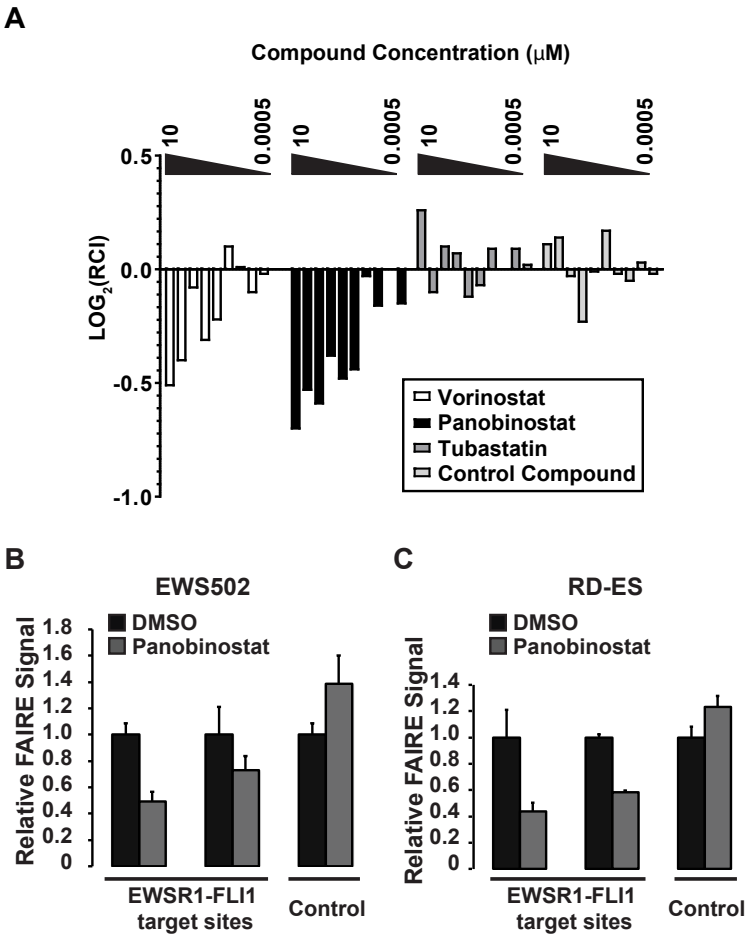

Figure 2.9: HDAC inhibition selectively decreases chromatin accessibility at EWSR1-FLI1 binding sites. (A) HT-FAIRE-qPCR at the same genomic regions used for the original screen was conducted after treatment of EWS894 cells for 16 h with threefold dilutions of Vorinostat, Panobinostat, Tubastatin, or a control compound in concentrations ranging from 10 to 0.0005 μM. Error bars represent the SE of two biological replicates with two technical replicates each. FAIRE-qPCR at EWSR1-FLI1 target sites and control site after Panobinostat treatment of (B) EWS502 or (C) RD-ES cells. EWSR1-FLI1 targets sites were P1 and P7 for B and C. Control FAIRE site was AURKAIP1 for B and C. All treatments were at 10 μM for 16 h unless otherwise noted. FAIRE is plotted relative to DMSO control and error bars represent the SD of three replicates.

To explore the mechanism underlying the chromatin signature reversal, we asked whether EWSR1-FLI1 levels were affected by HDAC inhibitor treatment. Panobinostat and Vorinostat treatment resulted in a dose-dependent decrease in *EWSR1-FLI1* mRNA levels, while Tubastatin had no effect (Fig. 2.10A). Consistent with the decrease in mRNA, EWSR1-FLI1 protein levels were also decreased following treatment with Panobinostat and Vorinostat (Fig. 2.10B). Tubastatin did not affect EWSR1-FLI1 protein levels although a slight overall decrease was noted at 10 μM (Fig. 2.10B). These data suggest that Panobinostat and Vorinostat, both hit

compounds identified in the HT-FAIRE screen, decrease levels of EWSR1-FLI1 by altering transcription.

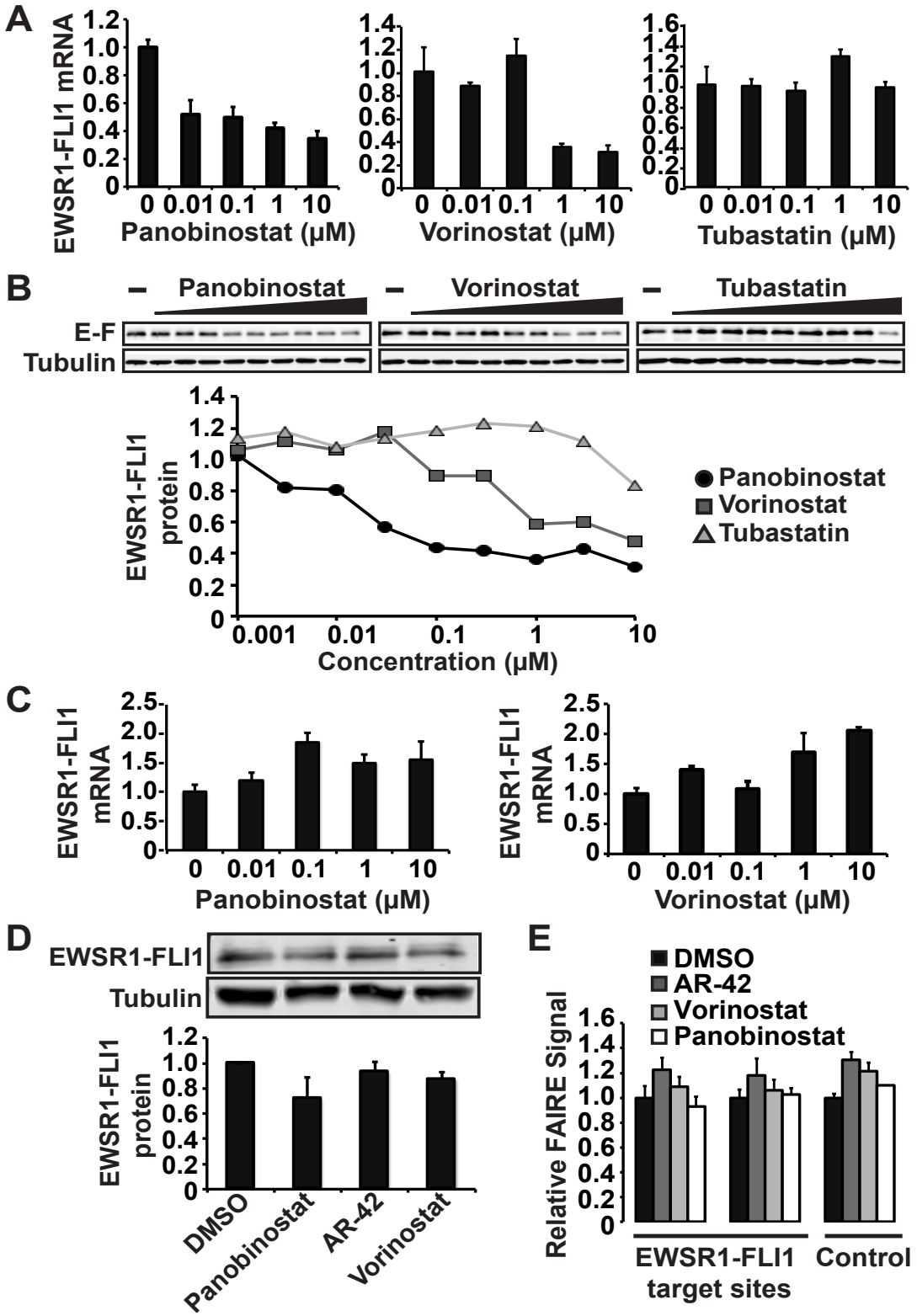

Figure 2.10: EWSR1-FLI1 mRNA and protein levels are decreased after HDAC inhibition. (*A*) EWSR1-FLI1 mRNA levels were measured by qRT-PCR after treatment of EWS894 cells with indicated concentrations of Panobinostat, Vorinostat, or Tubastatin. (*B*) EWS894 cells were treated with varying concentrations of Panobinostat, Vorinostat, or Tubastatin (threefold dilutions, 10 μM to 0.001 μM). Cell extracts were assayed for EWSR1-FLI1 ("E-F") and tubulin protein levels by immunoblot. All treatments were for 16 h. (*C*) EWS894 cells lentivirally transduced with EWSR1-FLI1 were treated with varying concentrations of Panobinostat or Vorinostat. RNA was measured by qRT-PCR. (*D*) Transduced EWSR1-FLI1 protein levels were measured in EWS894 cells after treatment with HDAC inhibitors (10 μM) by immunoblotting. (*E*) FAIRE-qPCR measuring chromatin accessibility in EWS894 cells with exogenous EWSR1-FLI1 after treatment with 10 μM multiple HDAC inhibitors. All treatments were for 16 h. Error bars represent the SD of three technical replicates (*C* and *E*) or three biological replicates (*D*).

We then asked whether ectopically expressed EWSR1-FLI1 would be similarly affected by HDAC inhibition. We generated a Ewing sarcoma cell line in which the endogenous EWSR1-FLI1 was silenced with concurrent stable expression of lentivirally transduced EWSR1-FLI1. Panobinostat or Vorinostat treatment of these cells did not affect *EWSR1-FLI1* mRNA levels (Fig. 2.10C). Correspondingly, treatment with multiple HDAC inhibitors had virtually no effect on exogenous EWSR1-FLI1 protein levels (Fig. 2.10D), in contrast to the endogenous protein (Fig. 2.11A). These data demonstrate that HDAC inhibition acts through transcription of the *EWSR1-FLI1* without affecting protein stability.

We then tested chromatin accessibility in the EWSR1-FLI1-transduced Ewing sarcoma cells. Treatment with multiple HDAC inhibitors failed to affect FAIRE signal at oncogene-targeted regions (Fig. 2.10E). These results were replicated in a second Ewing sarcoma cell line (EWS502) that similarly ectopically expresses EWSR1-FLI1 (Fig. 2.11B). Taken together, these data imply that the loss of chromatin accessibility at EWSR1-FLI1 binding sites results from HDAC inhibition-mediated alterations in EWSR1-FLI1 transcription, thereby suppressing oncoprotein levels, rather than HDAC activity directly at the chromatin target sites.

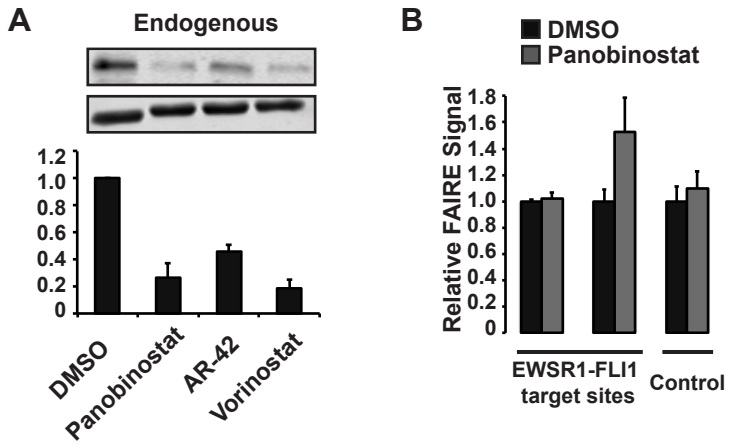

Figure 2.11: Chromatin effects of HDAC inhibition are dependent on HDAC-mediated transcriptional changes. (A) Endogenous EWSR1-FLI1 protein levels were measured in EWS894 cells after treatment with HDAC inhibitors (10 μM) by immunoblotting. (B) FAIRE-qPCR EWS502 cells with exogenous EWSR1-FLI1 treated with 10 μM Panobinostat. EWSR1-FLI1 targets sites were P1 and P7, and control FAIRE site was AURKAIP1. All treatments were for 16 h. Error bars represent the SD of three biological replicates (A) or three technical replicates (B).

2.4: Discussion

We have adapted and validated FAIRE as a high-throughput, automated assay for chromatin accessibility. Applying this method to screen a chromatin-focused chemical library enabled the identification of compounds that alter a disease-specific chromatin signature. Based on this screen we demonstrated a role for HDACs in the transcription of the central oncogenic protein, EWSR1-FLI1, thereby defining a potential chromatin regulatory mechanism involved in Ewing Sarcoma.

In contrast to previous efforts to inhibit EWSR1-FLI1 activity that have capitalized on individual target gene expression or physical interactions (67–70)the application of HT-FAIRE offered a strategy to identify therapeutics based on variation in chromatin accessibility, a universal genomic feature determined by the combined effects of transcriptional regulators and chromatin regulatory proteins (71). Unlike chromatin immunoprecipitation (ChIP), FAIRE does

not depend on the prior selection of a specific target. Without the need for an enzymatic processing step, FAIRE does not require the optimization (and consequent variability) associated with DNase, MNase, or Assay for Transposase-Accessible Chromatin (ATAC) (3) other techniques that explore chromatin accessibility. A specific chromatin signature associated with multiple molecular mechanisms can form the basis for an HT-FAIRE functional screen.

The connection between HDAC activity and *EWSR1-FLI1* had been noted previously. Romedepsin, also a hit in our screen, had been shown to decrease *EWSR1-FLI1* mRNA levels and also had a profound anti-proliferative activity on Ewing cells (72). In a separate study, Vorinostat treatment reversed the EWSR1-FLI1-mediated transcriptional activation signature in Ewing sarcoma cells but not the repressive gene signature. Our data are consistent with these findings since HDAC inhibition primarily affects those genes regulated by EWSR1-FLI through the GGAA-containing microsatellite repeats, a relationship associated with gene activation. Indeed, our screen focused on these microsatellite regions.

The role of HDAC activity in transcription is complex. HDAC proteins are the catalytic subunits of multiple co-repressor complexes including Sin3A, NuRD, NCoR/SMRT, and CoREST (73). Recent evidence suggests the SP1 transcription factor directly binds to the *EWSR1-FLI1* promoter and positively regulates transcription. Although SP1 has been shown to interact with HDAC1 and HDAC2, this interaction mediates repression, in contrast to the activity noted in this study (74). HDAC-containing complexes are also known to function in transcriptional elongation and may selectively affect highly expressed genes in cancers (75).

In conclusion, we developed an approach to screen compounds based on changes in chromatin. HT-FAIRE is applicable to any cellular model associated with a specific chromatin accessibility signature and offers a general strategy to disrupt the function of proteins lacking

structure amenable to small molecule targeting or the absence of complete characterization of the biochemical pathways and partners. The chemical probes identified by this method can offer mechanistic insights into chromatin dysregulation in disease, lead to the identification of valid molecular targets, and serve as starting points for drug discovery efforts.

2.5: Methods

Cell Culture and Western Analysis.

EWS894 and EWS502 cells (76) were cultured in RPMI-1640 supplemented with 15% (vol/vol) FBS and maintained at standard growth conditions of 37 °C and 5% CO_2. Proteins were extracted using 2× Laemmli buffer, were separated by SDS/PAGE, and were then transferred onto nitrocellulose and probed for EWSR1-FLI1 (ab15289; Abcam) or tubulin (T9026; Sigma) and fluorescent secondary antibodies and quantified (LiCor).

Standard FAIRE, HT-FAIRE

FAIRE for sequencing was as follows: Replicate samples of chromatin from 2×10^7 cells were divided. Equal portions were used for standard FAIRE, as described or HT-FAIRE, using a ChIP DNA clean and concentrate column (11-379; Zymo Research) as per the manufacturer's instructions. FAIRE DNA from both replicates was prepared as per the manufacturer's recommendations (TruSeq DNA Sample Prep Kit; Illumina), and 50-bp reads were sequenced (HiSeq 2000; Illumina) at the University of North Carolina High-Throughput Sequencing Facility. Cells in a 96-well format were incubated for 16 h with compound or vehicle at a final concentration of 10 μM. After formaldehyde cross-linking, cells were sonicated in Lysis Buffer A. Input was collected from untreated cells in the first column of each plate, and FAIRE was

performed on remaining samples using columns (D5207; Zymo Research). Relative chromatin inhibition was determined by performing qPCR on FAIRE and input samples.

Analysis of Standard FAIRE and HT-FAIRE.

FAIRE data from seven cell lines (H1-hESC, HeLa, HepG2, NHEK, K562, GM12878, and HUVEC) were generated previously (77). For all signal-based analyses, one replicate was used for all cell lines except HUVEC, for which data from both replicates were used in parallel. Published sets of FAIRE sites were used in all cases. For HT-FAIRE, data from both replicates were combined, and one set of FAIRE sites was called using MACS2 (78) with a shift size set to 100. For hierarchical clustering analyses, we computed normalized FAIRE signal in 500-bp nonoverlapping windows across the genome. Windows were first filtered for those with an average signal greater than 0.25 (581,514 windows remained) and that fell within an expected range (580,605 windows remained). Windows exhibiting a wide variation across samples (SD greater than 0.5; 9,711 windows remained) were then selected. Signal in these windows was then median-centered and hierarchically clustered using average linkage. ChIP-seq data for histone modifications and transcription factors, as well as DNase hypersensitivity, were generated previously (77). Repetitive element classes were as defined by RepeatMasker, and genomic redundancy was computed for 36- and 50-bp reads using PeakSeq (79). Motifs in clusters 1–3 were identified using HOMER (80) using the 500-bp flanking sequence as background. Motifs were considered significant if they had a q-value equal to 0, they occurred in >20% of the target sequences, and had a greater than threefold enrichment in the target sequences relative to flanking sequences (background). Motifs in the same transcription factor family were merged for simplicity of presentation.

Detailed Description of High-Throughput FAIRE Screen

The automated, high-throughput FAIRE screen was performed in a 96-well format. Compound and vehicle controls were used in the assay at a final concentration of 10 μM in 0.1% DMSO in cell culture media. Compounds were plated onto a 96-well V-bottom cell culture plate (651180; Greiner Bio-One), and EWS894 cells were added (Multidrop Titertek) at 1×10^5 cells per well in a 100-μL final volume of cell culture media (RPMI supplemented with 15% FBS). Cells were incubated with compound for 16 h at 37 °C and 5% CO_2 and then harvested. Formaldehyde diluted in cell culture media to a final concentration of 1% per well was added (Multidrop Titertek). Plates were incubated for 5 min at 37 °C and 5% CO_2, followed by addition of glycine to a final concentration of 125 mM and incubation at room temperature for 5 min. Plates were centrifuged for 5 min at 500 × *g* (5810R centrifuge; Eppendorf) to pellet the cells. Media were removed by quickly inverting the plate. Cells were washed once with PBS and pelleted. A Tecan Evo 200 was used for all subsequent liquid handling. Cells were suspended in 50 μL of Lysis buffer A (57) and transferred to a 0.2-mL 96-raised well PCR plate (27-105; Genesee Scientific) for sonication. The plates were sealed with a 96-well silicone sealing mat (22-513; Genesee Scientific), and a pin lid was pushed through the seal (SL0096-P21-SS; Matrical Bioscience). Plates were sonicated (SonicMan; Matrical Bioscience) for 20 cycles for 15 s at 60% power. Then, 700 U of RNase (2900142; 5 Prime) was added to each well and incubated for 5 min at room temperature. Untreated samples from the first column of the plate were removed and pooled for input DNA. The input sample was digested with 20 μg of proteinase K at 55 °C overnight and then purified by phenol-chloroform extraction. FAIRE was performed by transferring liquid from the remaining wells in columns 2–12 to a ZR-96 ChIP

DNA silica matrix clean and concentrator column (D5207; Zymo Research). The column was then washed according to the manufacturer's instructions using a QiaVAC 96 (19504; Qiagen). DNA was eluted in a 100-μL Elution Buffer (Zymo Research). DNA was separated on a 1.5% agarose gel to confirm fragmentation. Ten microliters of the remaining input was diluted 1:1,000 and added back to the plate containing the FAIRE DNA. Buffer alone was also added to the plate as a control for qPCR. Two microliters of each sample was transferred from the 96-well plate to a 384-well plate for use in qPCR. Input samples were diluted 1:1,000, and FAIRE samples were diluted 1:100 in water for comparison of standard and HT-FAIRE. Input samples were diluted 1:1,000, and FAIRE samples (100-μL elution volume) were used undiluted for the HT-FAIRE screen. Two microliters of each diluted sample was subjected to quantification qPCR in duplicate on the ABI 7900HT using FastStart SYBR Green Master Mix ROX (Roche) in a 10-μL final volume. Primer sequences are listed in Table 2.3. Percent input was determined using the ΔCt method (76) . For the comparison of phenol-chloroform and column-based FAIRE methods, ΔCt values were normalized to a genomic region near the PRPF31 gene that is negative for FAIRE signal. For the FAIRE screen, relative chromatin inhibition was calculated using the following equation: (((ΔΔCt*P1*/ΔΔCt*AURKAIP1*) + (ΔΔCt*P7*/ΔΔCt*AURKAIP1*))/2), where P1 and P7 are EWSR1-FLI1–dependent open chromatin regions, AURKAIP1 is a region of chromatin that consistently has a positive FAIRE signal, and ΔΔCt is (FAIRE Ct*TREATED*/Input Ct*TREATED*)/(FAIRE Ct*DMSO*/Input Ct*DMSO*).

Name	Oligo Sequence
AURKAIP1 Forward (postive control)	TATACCCGCAGGTCCAGAATCGTT
AURKAIP1 Reverse (positive control)	AATAGCTCTAGACGCTTCCGCCTT
BC006361 Forward (negative control)	TTCTCCAACTTTGGAAGCCCAGGA
BC006361 Reverse (negative control)	TGTCTCCTTCTAGGCCCTCACAAT
P1 Forward (EWSR1-FLI1 binding)	AAGGAAGGAAGGGAGGGACACATAC
P1 Reverse (EWSR1-FLI1 binding)	CCTGTGAGTGTGACAGATTACTTGG
P7 Forward (EWSR1-FLI1 binding)	GGGTGACAGAGTAAGATCCTGTCAGA
P7 Reverse (EWSR1-FLI1 binding)	TGGGCGTGGTTCTCATGT
Enhancer1 Forward	TCCTGACTCACTGCCTGGAGCAT
Enhancer1 Reverse	GGGATTCCTGGAGTCACGGCA
Enhancer2 Forward	GGCTCAAGCGCCTGGGTTTTGTA
Enhancer2 Reverse	CAGCGTGGCTTCCTGGGCTTC
Enhancer3 Forward	TTGCAAGTGAGTAAGCAGAAGCCCA
Enhancer3 Reverse	AGCTGACCTCTCCCCTGTGTTAGT
Enhancer4 Forward	AGTGTGGCGCCGCTCTGGTT
Enhancer4 Reverse	CGTATTTGGCCACAGGAGGGAGC
Enhancer5 Forward	ACGGCTGATCGTGTGACTTTCTGC
Enhancer5 Reverse	GCCTTGACCAACTTGCTGAGGAGT
Negative1 Forward	GTGGGAAGCTATGGCTGAGAAGCA
Negative1 Reverse	TTGCCTTGGATTCCGTGCAGC
Negative2 Forward	ACAGCCGGGGCAACTAGAAGA
Negative2 Reverse	GACACCGCTTGGACCCGAGG
Negative3 Forward	CCAGCTTGTCATGGCTACAGGGC
Negative3 Reverse	GCTCACCGCAGTGACTCAGCAG
Negative4 Forward	AGGTCAGCGTCAAAGAGGGGCT
Negative4 Reverse	ACCTGACGCATGAAGGGCAGC
Negative5 Forward	AGAGCCAAACCCAAGGAGGTAACTA
Negative5 Reverse	GCCCACATGCATGCAATCCCA
Promoter1 Forward	CGGGAGGCCAATCGAACGCC
Promoter1 Reverse	GCTGAACGTCGCTCCTGACCC
Promoter2 Forward	GCACCTCCCTCTGCCGCTTC
Promoter2 Reverse	GCCCTCAAAGGGGCGGAACC
Promoter3 Forward	ACTGCGTCGCTGGCTTGGAG
Promoter3 Reverse	AAACGCGTGCCCAGCCAATCA
Promoter4 Forward	GGAACAGATGAGGCAGGCAGGG
Promoter4 Reverse	TTCTTTCCTCCTCTTTTTGCGGTGG
Promoter5 Forward	GTGAGAGTGCAGGGCCCCAAG
Promoter5 Reverse	GCCCGCCTTTCTCGCCGGTA
Promoter6 Forward	TCACATGACCCGCCCAACCG
Promoter6 Reverse	CGACGGCGGAAGAGAACGCT
Target 3 Forward	GCATCAGGAAGCCTGGATCCATTA
Target 3 Reverse	GTATATACCAACACCCTTCCCTG
Target 4 Forward	AGATCCGGTTCAAATGGCAAGAGC
Target 4 Reverse	GCACTCATCCTTAAGCCTCAACCA
Control 2 Forward	CAAACTTCGGCTCACTTCGGCAAT
Control 2 Reverse	AAGAAAGCCGAAACATGTCGCTCC
EWSR1-FLI1 mRNA Forward	GCTATGGTCAACAAAGCAGCTATG
EWSR1-FLI1 mRNA Reverse	TTGGCTAGGCGACTGCTGGT
RPL27 mRNA Forward	GACGCAAAGCTGTCATCGTG
RPL27 mRNA Reverse	GCAGTTTCTGGAAGAACCAC

Table 2.3: Primers used for FAIRE- and RNA-quantitative PCR

RNA Extraction

RNA was extracted (74134; Qiagen) followed by cDNA synthesis (Superscript III; Invitrogen). Ten microliters of qPCR reactions (SYBR Green Mastermix; Bio-Rad or Biotool) were performed according to the manufacturers' instructions. qPCR for FAIRE and cDNA was performed (ViiA7 Real-Time PCR system; Applied Biosystems) and analyzed using the ΔΔCt method (76).

Chapter 3: UNC0621 is a novel small molecule inhibitor of chromatin accessibility in Ewing sarcoma

3.1: Introduction

In addition to HDAC inhibitors, the automated FAIRE screen led to the identification of many small molecule compounds that decreased chromatin accessibility at EWSR1-FLI1 binding sites. The majority of these compounds, indicative of the composition of the EpiG library, were designed as inhibitors towards specific proteins but possessed yet-to-be-determined biological function and targets. One such compound, UNC0621, appeared to be a particularly potent inhibitor of chromatin accessibility (Fig 3.1). This compound was intriguing because it is an analog of UNC0638, a well-characterized inhibitor of the G9a/GLP histone methyltransferases (51). UNC0638 was included in the EpiG library, but caused a negligible effect on chromatin accessibility in the screen. This led to supposition that UNC0621 was in fact acting on chromatin through an undetermined secondary target and mechanism.

To begin to explore the mechanism of action of UNC0621 in Ewing sarcoma cells, we compared its function to that of the previously studied HDAC inhibitors. As we found HDACi decreased chromatin accessibility through a decrease in EWSR1-FLI1 protein levels, we asked whether UNC0621 caused the same effect. Upon analyzing EWSR1-FLI1 protein levels following treatment of EWS894 cells with UNC0621 for 16 hours, we observed no significant difference in proteins levels of treated cells relative to a vehicle control (Fig 3.2A-B). This indicated that UNC0621 was not influencing chromatin by altering oncoprotein levels.

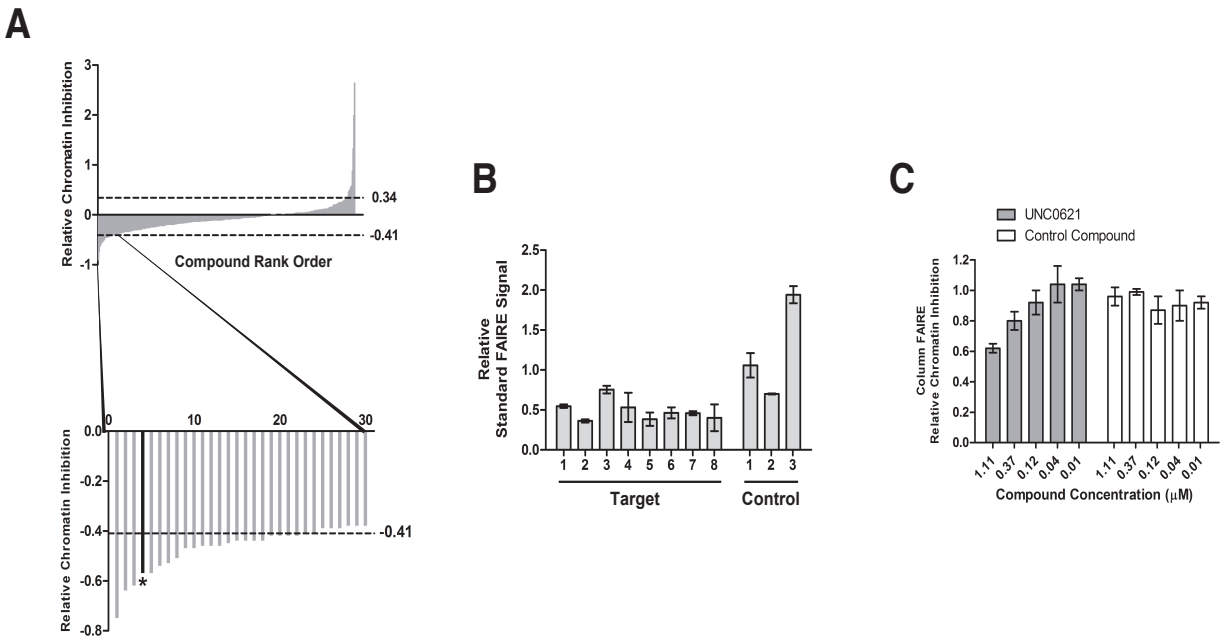

Figure 3.1: Chromatin signature-based screen identified UNC0621 as an inhibitor of EWS-FLI-dependent chromatin accessibility. **(A)** $\log_2$ ratio of the relative chromatin inhibition values was plotted against the rank order of compounds from greatest relative decrease (top, left side of X-axis) to the greatest relative increase (top, right side of X-axis) in FAIRE signal following compound treatment. The dashed lines indicate the significance cutoff of relative chromatin inhibition values greater or less than two standard deviations from the average FAIRE signal for vehicle-treated controls. Thirty compounds that show the greatest decrease in FAIRE signal for each plate are magnified (bottom graph). The bar representing UNC0621 is highlighted in black with an asterisk (*). (**B**) Standard FAIRE-qPCR at 11 genomic loci known to be enriched by FAIRE in EWS894 cells following 16-hr treatment with 10 μM UNC0621. "Target" sites were dependent on the binding and presence of EWS-FLI1 for a positive FAIRE signal, whereas "Control" sites were not EWS-FLI1-dependent. Error bars represent the standard deviation of three biological replicates. **(C)** HT-FAIRE-qPCR at the same genomic regions used for the original screen was conducted following treatment of EWS894 cells for 16 hours with 3-fold dilutions of UNC0621 or a control compound in concentrations ranging from 1.11 to 0.01 μM. Error bars represent the standard deviation of 4 replicates for UNC0621 and the standard error of 2 replicates for the control compound.

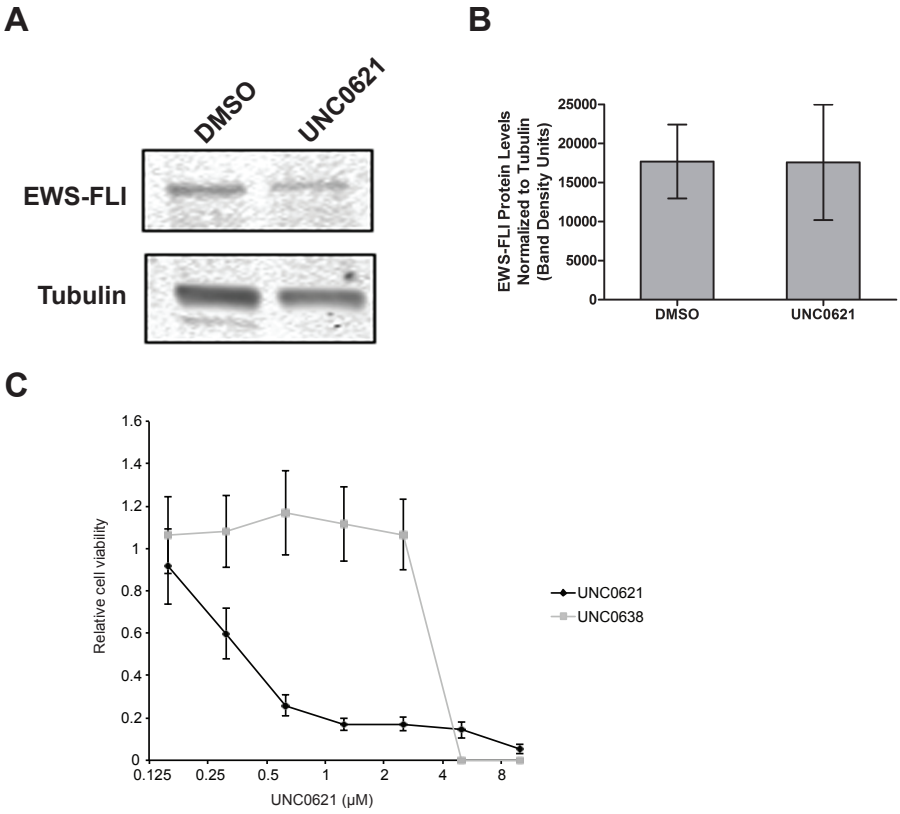

Fig 3.2: UNC0621 functions via a mechanism distinct from HDAC or G9a inhibitors. (a) EWS894 cells were treated with 10 μM UNC0621 for 16 hours, followed by western blotting with whole cell extract. **(b)** EWSR1-FLI1 and tubulin bands were quantified (LiCor) and plotted as a ratio. (c) Cell viability was assayed using WST-1 reagent (Roche) and spectrophotometry. Background absorbance (620 nm) was subtracted from assay absorbance (450 nm) values. Relative cell viability is expressed as $Compound^{Abs450-620}/DMSO^{Abs450-620}$.

Seeking to understand the effect of UNC0621 on Ewing sarcoma cells, we asked whether treatment with the compound affected cell viability. To measure cell viability we used WST-1, an assay that involves the conversion of WST-1 to formazan by NADH+ produced by respiring cells, resulting in a color change. A darker color, quantified by absorbance, indicates more NADH+ and correlates with more viable cells. We treated EWS894 cells with a 2-fold serial

titration of UNC0621, concentrations 10 μM to 0.156 μM, and performed a WST-1 assay 72 hours after treatment to measure cell viability. Interestingly, we observed that treatment with UNC0621 caused a dose-dependent decrease in the cell viability of EWS894 cells, with an EC_{50} of about 600 nM. Moreover, the published G9a inhibitor UNC0638 has a far less potent effect on cell viability, with an EC50 of about 3 uM. The potency of UNC0621 on decreasing both chromatin accessibility and cell viability suggested this compound was potentially targeting cancer-relevant epigenetic processes.

3.2: Generation and testing of UNC0621 derivatives

In order to study the mechanism of action of UNC0621, we needed a system to identify direct interactions with the compound. We desired a "handle" on the compound that could be attached to various moieties and used for compound interaction studies. Kyle Butler and Jian Jin (Mt. Sinai School of Medicine) generated compound derivatives possessing a short alkene linker. The resulting analogs, UNC4151 and UNC4152, possess the same structure as UNC0621 save for the addition of a short carbon linker and alkene (Fig 3.3A). The derivatives are distinguished by the location of the linker. Multiple derivatives were generated in order to determine the best location for the linker that would have the least impact on the function of the small molecule.

To determine whether the alkene linker affected compound activity, we compared the function of the new analogs to that of the parent compound UNC0621. First, we examined how the compounds affect chromatin accessibility by treating EWS894 cells with varying doses of each compound for 16 hours followed by the FAIRE assay. As previously shown, UNC0621 caused a marked and dose-dependent decrease in chromatin accessibility at EWSR1-FLI1 target sites (Fig. 3.3B).

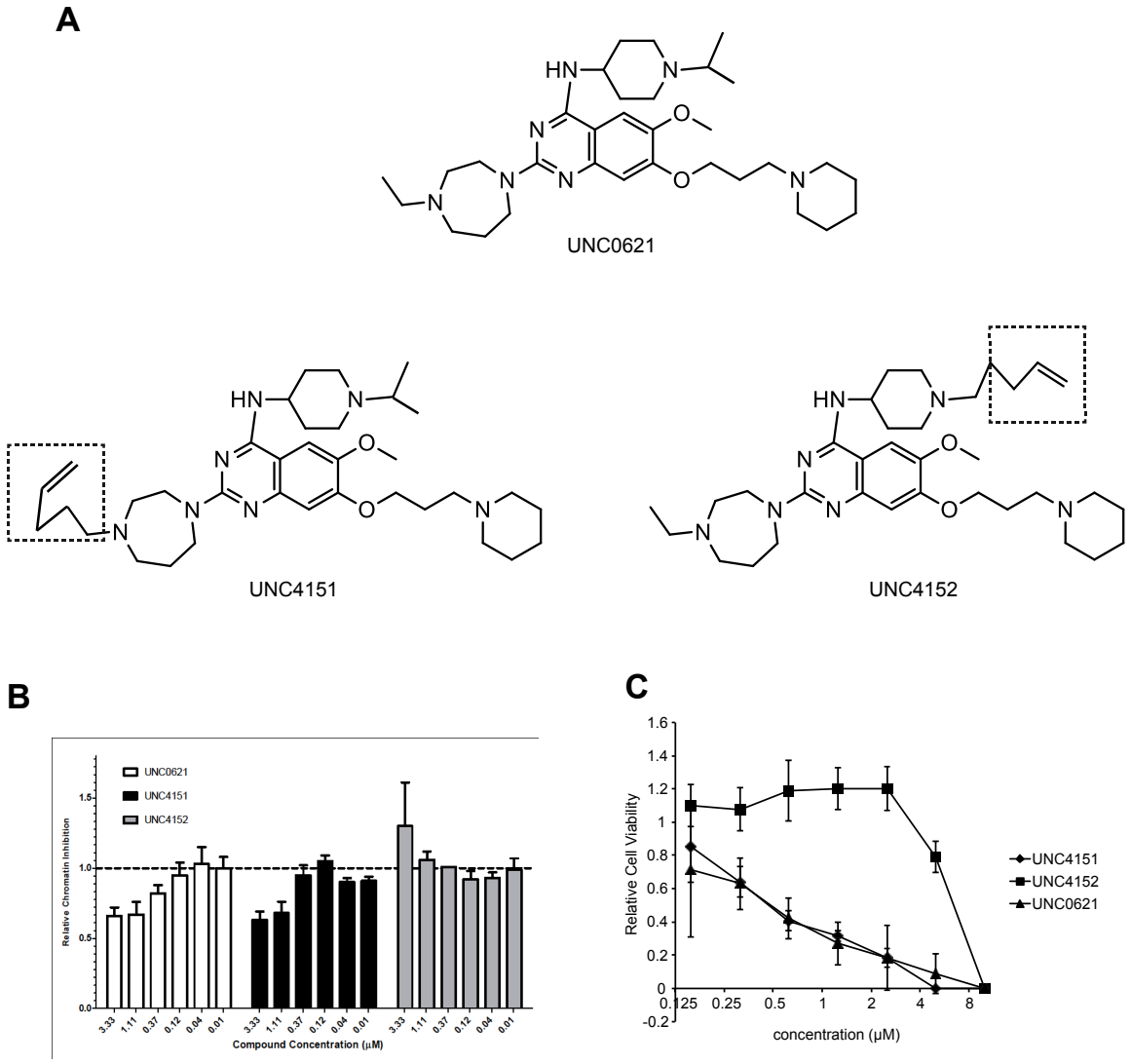

Fig 3.3: UNC0621 derivatives differ in their in biological activity. A) Structure of UNC0621 and derivatives UNC4151 and UNC4152. B) FAIRE-qPCR performed on EWS894 cells treated with all 3 compounds, Relative chromatin inhibition score is a ratio of FAIRE signal at test regions (oncoprotein bound sites) and an unbound control. Error bars represent standard deviation of 5 technical replicates. C) Cell viability assay in EWS894 cells treated with UNC0621 and derivatives. Relative viability is plotted as absorbance relative to DMSO. Error bars represent standard deviation of 3 technical replicates.

Similarly, treatment with the UNC4151 analog caused a comparable decrease in chromatin accessibility at analyzed sites. Contrastingly, UNC4152 did not significantly affect chromatin accessibility relative to vehicle control. This indicates that the UNC4151 analog retains the chromatin modulating function of UNC0621, whereas this has been ablated in UNC4152.

To further compare the activities of the analog compounds to the parent UNC0621, we examined their effect on cell viability. UNC0621 had previously been demonstrated to decrease proliferation of Ewing sarcoma cells as measured by WST-1. We treated EWS894 cells with a 2-fold dose titration of all three compounds, from 10 μM to 0.156 μM, then measured cell viability by WST-1 72 hours after treatment. We observed that, as expected, cell viability decreased with increasing concentrations of UNC0621. UNC4151 treatment closely recapitulated UNC0621, exhibiting a similar effect on cell viability (Fig. 3.3C). However, UNC4152 exhibited an attenuated effect, with only the highest concentration (10 μM) resulting in a decrease in viability and the remaining concentrations causing no effect relative to vehicle control. Together with the FAIRE results, this suggests that UNC4151 functions similarly to UNC0621 whereas UNC4152 demonstrates perturbed function. Therefore, we conclude that the location of the linker in UNC4151 has negligible impact on compound activity and can be used to study potential interactions of UNC0621. Additionally, the disrupted activity of UNC4152 gave the potential for this derivative to be used as an "inactive" control compound and help eliminate biologically irrevelant interactions in future studies.

UNC4151, as well as "inactive" derivative UNC4152, were conjugated to NHS sepharose beads through the short carbon linker present in both compounds. The sepharose acts as a tether

that can be isolated in pull-down experiments, thereby allowing detection of factors interacting with the associated compounds.

3.3: UNC0621 derivative compounds interact with nuclear proteins

Having observed that UNC4151 possesses comparable biological activity to that of UNC0621, we then wanted to use this compound to study protein interactions of UNC0621 and identify potential molecular targets. Due to the initial discovery of UNC0621 as a chromatin-modulating compound, we hypothesized that the most relevant targets were likely nuclear proteins. To determine interaction of UNC0621 with nuclear proteins, we used the "active" derivative UNC4151 conjugated to sepharose as a proxy to detect relevant UNC0621 interactions. Additionally, we used regular NHS sepharose beads as a negative control and the "inactive derivative" UNC4152, also conjugated to sepharose, as a quasi-control probe with similar structure but disrupted activity. We hypothesized that nuclear proteins would be associated with bead-conjugated compounds, and that relevant interactions would exhibit greater association with UNC4151 than with UNC4152.

To determine nuclear protein interactions with bead-conjugated compounds, we isolate nuclear proteins from Ewing sarcoma cells and incubated with sepharose beads alone or bead-conjugated UNC4151 or UNC4152. Samples were then allowed to drip through the column, with interacting proteins remaining bound to beads. Bound proteins were eluted off with soluble UNC0621 followed by SDS-PAGE silver stain analysis. For both EWS502 and EWS894 cells, we observed peptides across a wide range of molecular weights were pulled down abundantly with both bead-conjugated UNC4151 and UNC4152 (Fig 3.4A). While there were also peptides

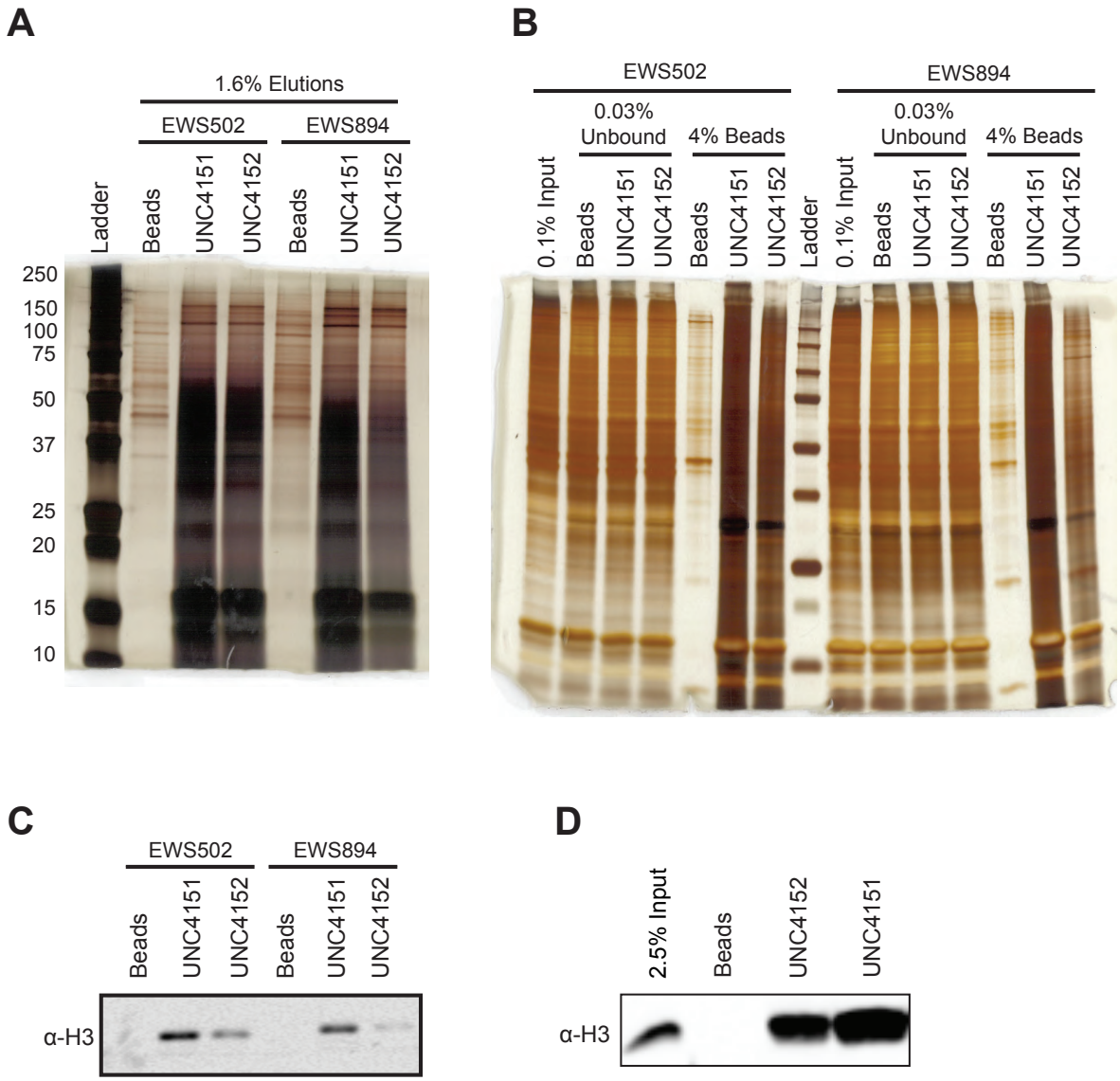

Fig 3.4: Bead-conjugated UNC0621 derivatives interact with histones and nuclear proteins. A) Silver stain analysis of nuclear protein pull-down with bead-conjugated derivatives. B) Silver stain analysis of proteins present in the flow through from nuclear pull-downs ("0.03% unbound") and proteins that remained associated with sepharose following pull-downs ("4% beads"). C) Nuclear protein pull-down samples show presence of histone H3 by western blot. D) Nucleosome pull-downs with bead-conjugated compounds show presence of histone H3 by western blot. Nucleosomes were isolated from HEK293T cells.

associated with the empty NHS sepharose beads, they were far less abundant, indicating that background binding to just the sepharose was reasonably low. Interestingly, although many peptides were associated with the inactive UNC4152, they were less abundant than the interactions with UNC4151. Because the binding reactions were controlled for initial protein concentration and small molecule molarity, it can be assumed that the observed difference in abundance is due to a difference in binding efficiency of the compounds. This agrees with our hypothesis that interacting proteins would associate more abundantly with UNC4151. Therefore, these data suggest that while the inactive derivative UNC4152 does interact with nuclear proteins, it does so with lower efficacy than UNC4151. This difference in interaction efficiency could potentially explain the severely perturbed, though not absent, biological function of UNC4152.

We wanted to determine whether there were nuclear proteins that were not captured in the compound pull-downs. To address this, we analyzed the portion of the lysate that had flowed through the chromatography column, and therefore had not bound to the sepharose. We analyzed the flow-through from all pull-downs by silver stain analysis and observed in all samples a high abundance of proteins across the entire range of molecular weights that had not bound to the sepharose. Surprisingly, although the eluted fractions varied, the unbound fraction of UNC4151 and UNC4152 pull-downs appeared equally as concentrated as that of the sepharose beads control.

Additionally, to address the efficacy of the elution with UNC0621, we asked what proteins were still associated with the sepharose beads following the protein pull-down.. We observed many proteins were still associated with the beads conjugated to UNC4151 and UNC4152, though the latter exhibited decreased overall associations. This indicated that elution

with free UNC0621, though somewhat effective, failed to liberate many proteins associated with bead-conjugated small molecules.

In analyzing the pattern of UNC0621 derivative-interacting proteins, we noticed the most abundant species was at approximately 16 kD. We hypothesized that these could be histones, with the rationale that histones have the same observed molecular weight and are very abundant within the nucleus. To address this, I performed a western blot to detect total levels of histone H3 in nuclear pull-down lysates. I observed that H3 was undetectable in the NHS sepharose negative control but was present in nuclear pull-downs from UNC4151 and UNC4152. Additionally, H3 levels are lower in the UNC4152 pull-down than with UNC4151, which is consistent with our previous observation that the UNC4152 pull-down has overall lower protein abundance than the pull-down with UNC4152. Therefore, UNC0621 interacts with histone H3 and this association is stronger with the active derivative compound than the inactive compound. In addition, the pull-downs were shown to be highly enriched for all histones by mass spectrometry (Amber Mosley, Indiana University).

Although histones were highly enriched by mass spectrometry, it could not be determined whether these interactions were in the context of a protein complex or more direct. To understand how UNC0621 engages histones, we asked whether UNC0621 could bind to nucleosomes. We generated a crude solution of mononucleosomes by isolating intact nuclei and treating with micrococcal nuclease (MNase). MNase is an endonuclease that digests the linker DNA between individual nucleosomes, thereby fragmenting chromatin into regular nucleosomal arrays. By using a high concentration of MNase, we are able to yield primarily mononucleosomes. We incubated the mononucleosomes with sepharose-conjugated UNC4151 and UNC4152, then harvested the sepharose beads and boiled to liberate bound proteins. Isolated

proteins were separated by SDS-PAGE and analyzed by western blot to detect total levels of histone H3. We detected high signal for H3 in nucleosome pull-downs for UNC4151 and UNC4152, and there was no detectable H3 isolated with the empty sepharose beads alone. Moreover, we again observed lower levels of H3 associated with inactive derivative UNC4152 than with UNC4151, further indicating that the former compound has decreased binding efficacy relative to the latter.

Derivatives of UNC0621 conjugated to sepharose beads have demonstrated great potential in detecting compound-specific interactions. We have shown that UNC0621 derivatives interact with a wide range of nuclear proteins, and these interactions are enriched for histone proteins. However, the unbound fractions corresponding to the nuclear pull-downs were concentrated, suggesting that the binding capacity of the sepharose-conjugated was exceeded and many proteins were excluded. Additionally, following elution with UNC0621 to remove bound proteins, many proteins remained bound to the sepharose. It is possible that this elution was lacking in efficacy. Therefore, development of a more effective elution strategy would likely increase the protein yield and assist in identifying additional relevant interactions.

In subsequent nucleosome pull-down experiments, we found that sepharose-conjugated UNC0621 derivatives pull-down histones, providing further evidence for engagement with nucleosomes by UNC0621. However, while the lysate was enriched for nucleosomes, other nuclear proteins are present. It must still be determined whether UNC0621 directly interacts with nucleosome particle directly or indirectly through other chromatin-associated proteins.

Elutes of proteins associated with the active derivative UNC4151 are more concentrated than those associated with the inactive derivative UNC4152, indicating that the inactive compound has decreased interaction efficiency. Since UNC4152 does still bind protein, it is

plausible that the decreased biological activity of this derivative is due to attenuated interactions rather than a complete loss of function. However, the difference in binding between UNC4151 and UNC4152 can be potentially useful in determining biologically relevant interactions of UNC0621.

3.4: UNC0621 derivatives bind to fragmented fixed chromatin with high affinity

UNC0621 was identified as a chemical modulator of chromatin accessibility in Ewing sarcoma cells. We examined protein interactions of UNC0621 by performing nuclear protein compound pull-downs followed by silver stain and mass spectrometry analysis, and we identified histones associated abundantly with UNC0621 derivatives. Taking together the biological effect of UNC0621 on chromatin and its apparent interaction with histones, we hypothesized that UNC0621 directly binds to chromatin. To explore this hypothesis, our goal was to perform a chromatin pull-down with a tagged derivative of UNC0621 and determine the abundance of associated chromatin, the affinity of the interactions, and genome-wide localization (ref).

First, we asked whether we could detect an interaction between chromatin and UNC0621. I developed a chromatin pull-down protocol adapted from protocols for ChIP, Chem-seq, and Chem-ChIP (83,84). All methods have comparable instructions on formaldehyde fixation of cells and chromatin fragmentation, with subsequent divergence on pulling down chromatin with an antibody or small molecule compound. For initial experiments, we utilized UNC0621 derivatives, UNC4151 and UNC4152, conjugated to sepharose beads. Sepharose-conjugated compounds were incubated with fragmented crosslinked chromatin from EWS894 to determine the compounds' association with chromatin. We then quantified samples to determine the amount of chromatin associated with compounds. We found that chromatin associated with bead-conjugated derivatives, and when compared to a parallel processed input control, saw that

each pull-down contained 5-10% of the starting material used for each pull-down reaction (Fig 3.5A). Moreover, chromatin pull-downs performed with NHS sepharose beads as a negative control only represented ~0.1% of the input chromatin amount. This demonstrates that background association of chromatin with sepharose alone is low, indicating that chromatin interacts selectively with sepharose-conjugated UNC0621 derivative compounds.

Possessing evidence that UNC0621 does in fact interact with chromatin, we desired to use a derivative compound we believed would increase detection specificity. We utilized a biotinylated UNC0621 derivative, KB-13-60, that can be pulled out with magnetic beads coated with streptavidin. The use of magnetic beads rather than sepharose allows for a more streamlined isolation process while the strength of the biotin-streptavidin interaction maintains efficiency. Moreover, we wanted to determine whether the amount of associated chromatin is proportional to the amount of compound used for a pull-down. The listed binding capacity of the streptavidin magnetic beads is 1.1-1.7 nmol of biotin per mg of magnetic beads, and the beads are at a concentration of 10 mg/ml. With the assumption that the binding capacity would only be slightly lower for a biotinylated small molecule compound, we calculated the binding capacity of 0.5 mg streptavidin beads (equal to 50 uL) to be approximately 0.5 nmol of KB-13-60. To effectively vary the concentration of KB-13-60, we used a maximum of 0.5 nmol KB-13-60 and kept beads constant at 0.5 mg. Avoiding saturation of the beads would ensure the accuracy in the variation of each concentration of KB-13-60.

To test the utility of KB-13-60 for detecting chromatin interactions, we incubated varying concentrations of the compound with fragmented chromatin followed by addition of streptavidin-coated magnetic beads to pull out KB-13-60 in complex with associated chromatin. We quantified the DNA from each pull-down reaction and found that amount of DNA isolated was

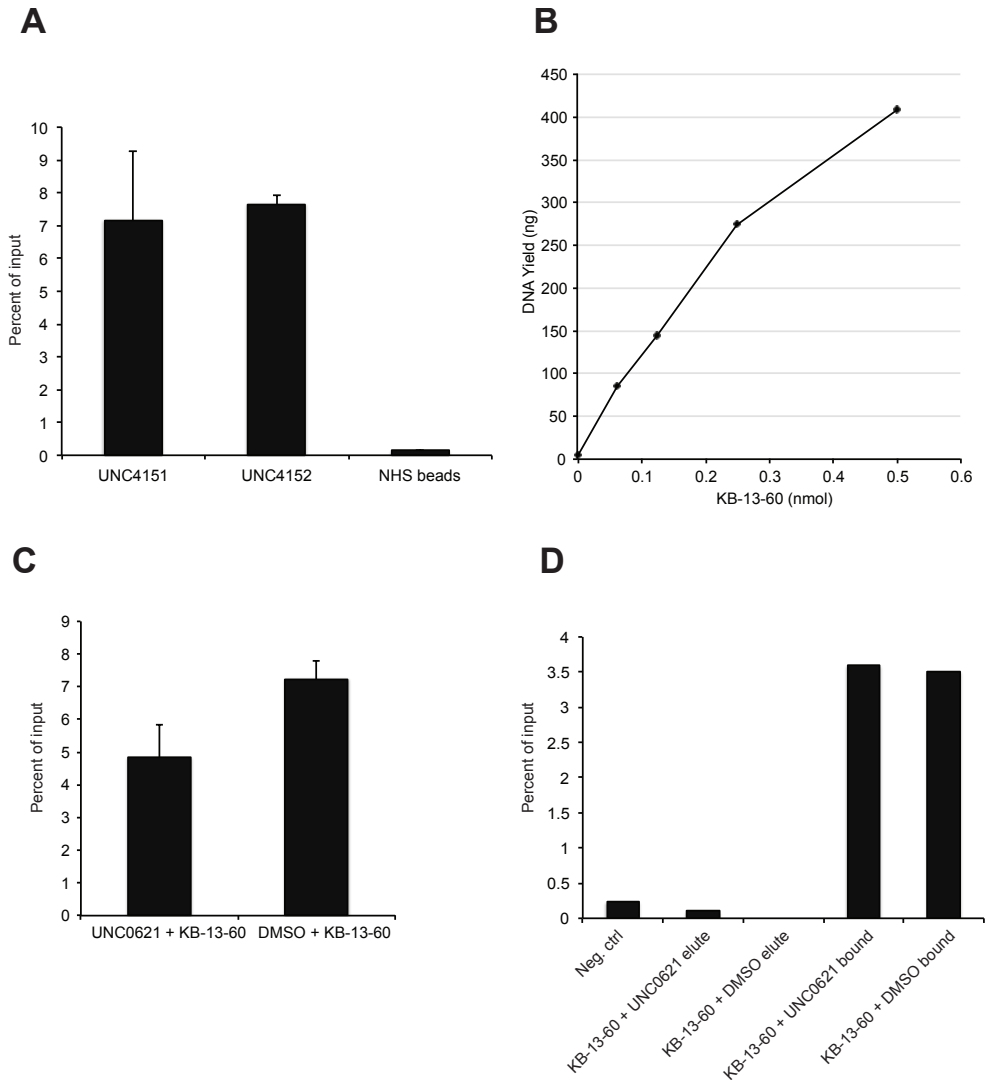

Fig 3.5: UNC0621 compound derivatives interact with fragmented chromatin. A) Chromatin pull-down using sepharose-conjugated compound derivatives. Values plotted as a percentage of an equivalent volume of not used for a pull-down ("input"). B) Representative chromatin pull-down using varying amounts of biotinylated derivative KB-13-60. Graph depicts total yield (ng) for each pull-down. C). Chromatin pull-down with 0.125 nmol KB-13-60 following pre-incubation of chromatin with either 5 nmol UNC0621 or DMSO. Error bars indicate standard deviation between 3 technical replicates. D) Representative experiment showing chromatin pull-down with KB-13-60 followed by elution with either UNC0621 or DMSO. DNA in the supernatant ("elute") and what remained associated with streptavidin beads ("bound") was quantified and plotted as a percentage of input.

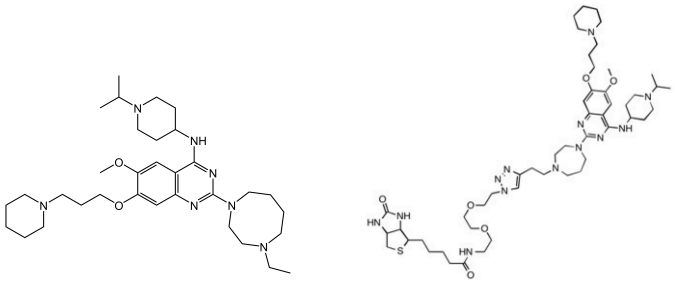

Fig 3.6: Structures of UNC0621 and its biotinylated derivative KB-13-60.
Synthesized by Kyle Butler and Jian Jin (Mt. Sinai School of Medicine)

proportional to the amount of KB-13-60 used for the pull-down, with the DNA yield dropping roughly two-fold with each two-fold decrease in compound concentration. This is further evidence of the specific interaction of chromatin with KB-13-60, and demonstrates quantitative nature of the interaction at compound concentrations below the binding capacity of the streptavidin beads. While the bead-conjugated compounds and KB-13-60 interact with similar efficacy, we can more easily and accurately titrate the amount of KB-13-60. Therefore, we chose to use KB-13-60 for subsequent chromatin interaction experiments.

Next, we wanted to understand the nature and specificity of the UNC0621-chromatin interaction. I hypothesized that if UNC0621 is indeed binding to chromatin, competition with free UNC0621 would occlude binding of KB-13-60 to chromatin. Since the interaction studies require the use of UNC0621 derivative compounds, competition experiments will permit interrogation of the binding properties of original UNC0621. To examine the ability of KB-13-60 to engage chromatin in the presence of UNC0621, I first incubated chromatin with UNC0621 or DMSO as a control then performed a chromatin pull-down with KB-13-60. Upon quantifying isolated chromatin, I observed that less chromatin was pulled down from reactions pre-incubated with UNC0621 relative to those pre-incubated with DMSO. DMSO-incubated pull-downs

averaged ~7% of input DNA, UNC0621-incubated samples averaged ~5% of input. While this difference was consistent, it represents only ~33% difference, indicating that KB-13-60 is still able to effectively bind to chromatin in the presence of UNC0621.

We also wanted to determine the ability of UNC0621 to compete off chromatin already bound to KB-13-60. To address this, we performed a chromatin pull-down with KB-13-60, then incubated the beads with wash buffer containing either UNC0621 or DMSO for 24 hours. Effective competition by UNC0621 would result in chromatin being present in the wash buffer rather than bound to KB-13-60 on the streptavidin beads. We quantified the DNA remaining on the beads as well as in the supernatant. In both UNC0621 and DMSO elution conditions, DNA in the supernatant was barely quantifiable and chromatin remained associated with streptavidin beads. Although UNC0621 is able to partially occlude binding of KB-13-60 to chromatin, under conditions tested UNC0621 cannot successfully compete for binding once KB-13-60 was already bound to chromatin. This suggests that KB-13-60 possesses the same binding targets as UNC0621, but KB-13-60 is able to bind chromatin more efficiently.

To explore the possibility of UNC0621 derivatives binding to the DNA component of chromatin rather that through a protein target as hypothesized, I performed a chromatin pull-down with KB-13-60 in the presence or absence of proteinase K. In the presence of proteinase K, interaction between chromatin and KB-13-60 is ablated (Fig 3.7A-B). This supports our hypothesis that UNC0621 derivatives associate with chromatin through a protein intermediate.

Chromatin pull-downs with KB-13-60 show that the compound has a high affinity for chromatin, as associated chromatin is not eluted effectively with UNC0621. To better understand the affinity of the compound for chromatin, we asked whether elution of compound-bound chromatin was affected by sodium chloride (NaCl) concentration. NaCl is known to disrupt

macromolecular interactions at high concentrations, particularly those with proteins. We hypothesized that increasing the concentration of NaCl would disrupt the protein target(s) of UNC0621 and consequently cause dissociation of chromatin from the compound. To assess the effect of NaCl concentration on the UNC0621-chromatin interaction, we performed a chromatin pull-down with KB-13-60 and incubated the compound-bead-chromatin complex with varying concentrations of NaCl. NaCl concentration ranged from 300 mM, the original concentration of the reaction buffer, up to 2 M. We incubated the beads with lowest concentration NaCl wash buffer, then removed a fraction of the bead solution and saved the supernatant as the "elution" for that NaCl concentration. Beads were subsequently incubated with the next highest concentration of NaCl, and another fraction was removed and supernatant retained. The process was repeated for each NaCl concentration in ascending order, with the same fraction of the starting amount removed after each incubation. Using this method, the quantity of each elution could be directly compared to each other. Moreover, each subsequent incubation is done with the same chromatin pull-down, allowing us to examine the relative contribution of each NaCl concentration on elution of KB-13-60-bound chromatin.

We quantified the eluted chromatin at each tested NaCl concentration as well as the chromatin that remained on the beads following all washes. A standard chromatin pull-down was prepared in parallel for comparison. 300 mM and 500 mM NaCl did not effectively elute chromatin off of beads, with quantified amounts in eluate lower than even the background control (Fig 3.7C). Elutions at 750 mM, 1 M, and 2 M NaCl exhibited higher concentrations of chromatin, at 1-2% of input quantity. Surprisingly, a significant amount of chromatin remained associated with streptavidin beads, about 5% of input relative to the ~4% that was eluted. Therefore, the majority of compound-associated chromatin remains on the streptavidin beads,

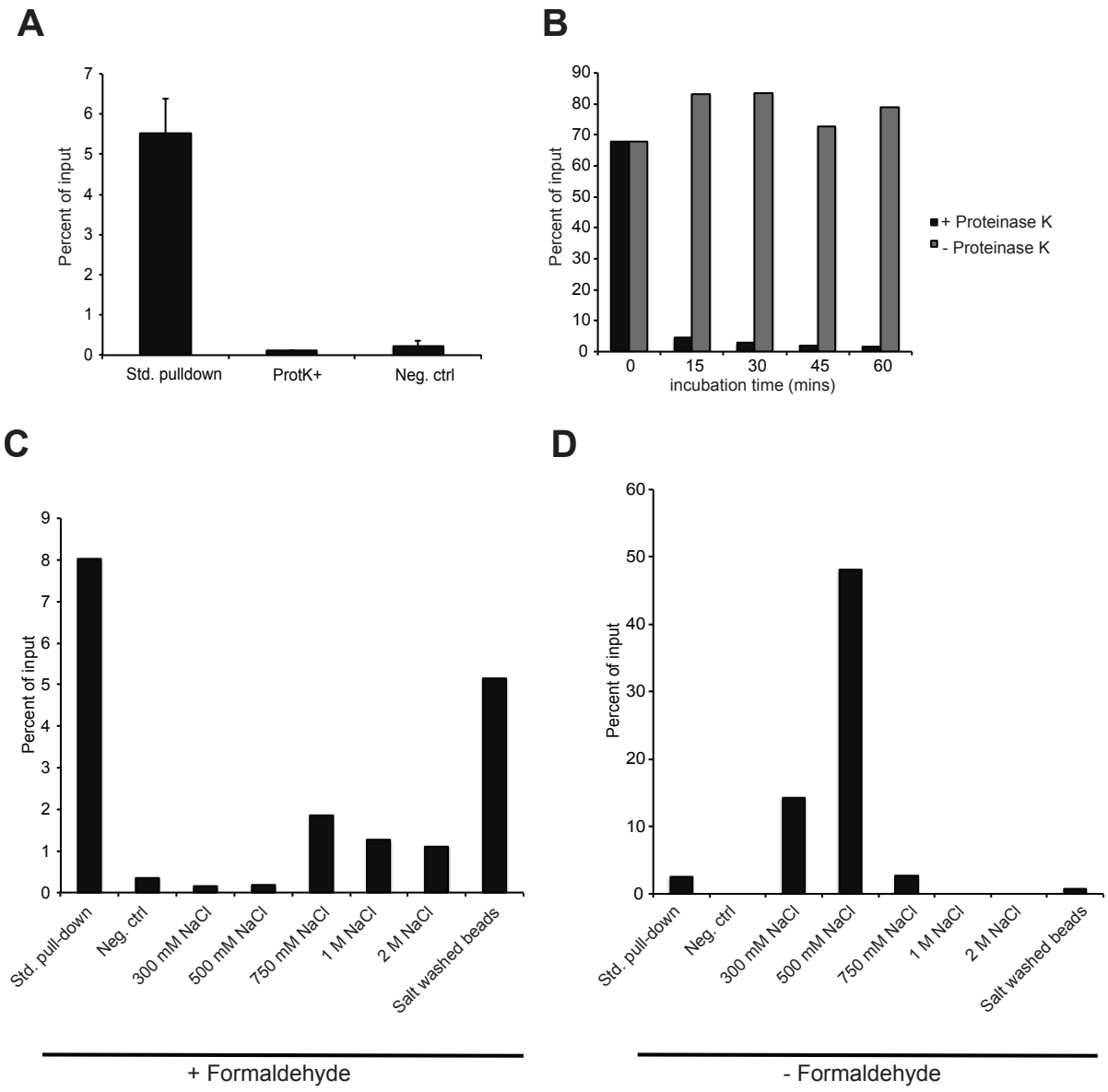

Fig 3.7: Cross-linking increases the affinity of KB-13-60 for chromatin. A) Pull-down with chromatin subjected to proteinase K treatment (ProtK+) prior to pull-down. A standard pull-down and negative control were performed in parallel and plotted for comparison. B) Representative experiment with proteinase K treatment for chromatin at varying time points prior to pull-down. Treatments were started at various times, each with a matched control, and all were stopped at the same time. Chromatin pull-downs performed in parallel. C) and D) Chromatin pull-down with elutions containing various concentrations of NaCl, with chromatin from either standard fixed EWS894 cells (C) or unfixed cells (D). Graphed is the chromatin quantified in each elution and remaining on the beads following all washes ("salt washed beads"). A representative pull-down is shown for each condition. Values on all graphs are plotted relative to an input control.

even after being washed with up to 2 M NaCl. This indicates that the affinity between KB-13-60 and chromatin is great enough to withstand high concentrations of NaCl.

We found it striking that 2 M NaCl was not sufficient to dissociate chromatin from KB-13-60. The apparent high affinity of this interaction led us to consider additional variables that were at play, in particular the inclusion of formaldehyde. Formaldehyde is included in the standard chromatin preparation and stabilizes protein interactions through cross-linking. Since UNC0621 appears to engage chromatin through a protein target, we asked whether the utilization of formaldehyde influences engagement of KB-13-60 with chromatin. To address this, I performed a KB-13-60 chromatin pull-down followed by salt elutions, as previously described, using chromatin from unfixed cells. Omitting the addition of formaldehyde, I isolated and fragmented chromatin from EWS894 cells and performed a chromatin pull-down with KB-13-60. Following binding of the compound to chromatin, I incubated the streptavidin beads with various concentrations of NaCl to elute bound chromatin. I then quantified the DNA present eluted at each concentration of NaCl and compared to the corresponding values obtained from fixed chromatin. I observed that the bulk of unfixed chromatin dissociates from KB-13-60 at 300 nM and 500 nM NaCl, with negligible amounts eluted at higher NaCl concentrations and remaining on the streptavidin beads after all washes (Fig 3.7D). This is in stark contrast to the quantities obtained with crosslinked chromatin, for which 300-500 nM NaCl liberates only negligible amounts of chromatin. These data suggest that crosslinking cells does in fact alter the affinity of the biotinylated KB-13-60 for chromatin. More specifically, KB-13-60 interaction with fixed chromatin is much more stable than with unfixed, and can withstand high concentrations of NaCl. Interestingly, the NaCl range that causes dissociation of KB-13-60 from unfixed chromatin is comparable to that at which the histone octamer dissociates (85). Therefore,

these findings are consistent with the observation that UNC0621 might bind histones or other nucleosome-bound proteins directly.

3.5: Discussion

Our studies with the tagged derivative compounds of UNC0621 have yielded valuable insights into the interactions of this compound with chromatin. We have shown that sepharose-conjugated compounds interact with nuclear proteins, in particular with histones. Because histones are a rather unconventional target, it is likely that there are other relevant protein targets of this compound. However, our elution by competition with equal molar UNC0621 was not the most effective, and therefore potentially interesting interactions could have been lost. Moving forward we are working on optimizing elution strategies and protein isolation approaches. The interactions of UNC0621 with histones and other proteins are being pursued in ongoing experiments.

Additionally, I have showed that biotinylated derivative compound KB-13-60 has high affinity for fixed chromatin and that this interaction is disrupted by competition with UNC0621. Importantly, I also showed that formaldehyde fixation increases the affinity of KB-13-60 for chromatin, stabilizing this interaction to the point of withstanding NaCl concentrations up to 2 M, which is exquisitely resistant. Histone proteins, due to their abundance throughout chromatin, would be highly crosslinked by formaldehyde. Therefore, if histones or histone-associated proteins are in fact a target of UNC0621, this could provide a potential explanation for the resistance of the KB-13-60-chromatin interaction to extremely high concentrations of NaCl. Formaldehyde fixation, although standard in ChIP/Chem-ChIP protocols, has emerged a major variable that influences our interpretation of how UNC0621 derivative compounds interact with

chromatin. While we now have an increased understanding of how KB-13-60 interacts with crosslinked chromatin, we now aim to perform interaction experiments using unfixed chromatin to eliminate the variable of formaldehyde. Another goal is to capture in vivo chromatin interactions using a compound derivative that, following treatment can be conjugated to biotin using click chemistry. This approach would be necessary as KB-13-60 does not appear to be cell permeable. Pilot experiments for these proposed methods are currently underway. Ultimately, these approaches will allow us to interrogate the interaction of UNC0621 derivative compounds with chromatin in a more native, biologically relevant context.

3.6: Methods

Standard FAIRE quantitative PCR

Cells were treated with 1% formaldehyde followed by inactivation with 125 mM glycine. Cells were resuspended in 2 ml of FAIRE lysis buffer (10 mM Tris-HCl pH 8, 2% Triton X-100, 1% SDS, 100 mM NaCl, 1 mM EDTA) and sonicated (Misonix Sonicator® 3000). Lysates were then subjected to organic extraction using phenol-chloroform to isolate nucleosome-depleted chromatin. Chromatin fragments were incubated with RNaseA for 30 min at 37 °C, proteinase K for 1 hour at 55 °C, followed by overnight crosslink reversal at 65 °C. FAIRE DNA samples were purified (Zymo DNA Clean & Concentrate columns, #11-379). Input control DNA was treated with RNaseA and proteinaseK prior to organic extraction.

qPCR reagents were combined in a 384-well plate in 10 µL reactions containing 5 µL of 2X iTaq™ Universal SYBR® Green Supermix (Bio-Rad), 3 µL of 1 µM primer pair mix, 1 µL of water, and 1 µL diluted DNA. qPCR was performed using ViiA™ 7 Real-Time PCR system (Applied Biosystems) and each region was analyzed using the ΔCt method, calculating the

FAIRE DNA quantification relative to the corresponding input control. The effect of UNC0621 treatment on each region was determined by $\Delta Ct_{UNC0621}$-ΔCt_{DMSO}.

Western blots

Proteins were extracted using RIPA lysis and separated by SDS-PAGE (Bio-Rad AnyKD™ SDS-PAGE gel, cat. No. 456-9035) then transferred onto nitrocellulose. Proteins were detected using fluorescent secondary antibodies, and quantified (LiCor). Antibodies as follows: α-Fli antibody (C-19, Santa Cruz sc-356, 1:1000), tubulin (Sigma T9026, 1:20,000), and histone H3 (from Strahl BD, 1:1000)

Nuclear protein pull-down with sepharose bead-conjugated small molecules

Nuclear proteins were isolated from EWS502 and EWS894 cells by cell lysis using Nuclei prep buffer to release intact nuclei followed by nuclei lysis. Nuclei were treated with Benzonase, a promiscuous exonuclease, to digest DNA and RNA, then ultra-centrifuged to isolate nuclear proteins. 50 uL Bead-conjugated UNC4151 and UNC4152, and NHS beads alone, were equilibrated with wash buffer in chromatography columns. Nuclear lysates were then incubated overnight in chromatography columns containing compounds. Samples were then allowed to drip through the column, with interacting proteins remaining bound to beads. Bound proteins were eluted off with soluble UNC0621 to compete off specific interactions. Elutions and remaining beads were boiled and proteins separated by SDS-PAGE, followed by silver stain analysis.

Nucleosome pulldown with sepharose bead-conjugated small molecules

Nucleosomes were prepared according to protocol adapted from Ruthenberg et al (86). Sepharose-conjugated compounds were diluted 1:10 in NHS beads, and 30 uL of this dilution was added to micro-centrifuge tubes and washed thrice with protein binding buffer (PBB) + 0.5% BSA to block beads. Prepared nucleosomes were added to micro-centrifuge tubes containing washed beads and rotate at 4C overnight. Compound-associated protein was collected by washing beads with PBB followed by resuspension of beads in 60 uL 2x SDS loading buffer. Sepharose beads were then boiled for 5 min to collect compound-associated proteins, which were then separated by SDS-PAGE and analyzed by western blot using antibody against histone H3.

Chromatin pull-downs with biotinylated KB-13-60

Chromatin was isolated from EWS894 cells and incubated with 0.125 nmol KB-13-60 in a 200 uL reaction volume for 2 hrs. MyOne T1 streptavidin-coated magnetic beads were added to reactions and incubated for 30 min. Bead-chromatin-compound complexes were then washed, then digested with RNaseA and proteinase K and boiled to reverse crosslinks and liberate compound associated chromatin. For input control, same volume of sonicated material used for pull-downs was immediate treated and RNaseA, proteinase K, and reversed crosslinks. Negative control reactions contained streptavidin beads with DMSO alone (no biotin).

Chapter 4: UNC0621 inhibits proliferation and oncogenic growth in Ewing sarcoma

4.1: Introduction

Ewing sarcoma cells exhibit aberrantly accessible chromatin at loci bound by the EWSR1-FLI1 oncoprotein. Accessible chromatin at these regions is likely necessary for EWSR1-FLI1 to activate an oncogenic transcriptional network. We identified UNC0621 as a modulator of chromatin accessibility in Ewing sarcoma cells and found treatment with this compound decreases chromatin accessibility at oncoprotein-bound loci. Because of the probable role of these regions in oncogenic growth, we sought to interrogate the effect of UNC0621 on the cell biology of Ewing sarcoma cells.

4.2: UNC0621 decreases viability of Ewing sarcoma cells

I previously observed that UNC0621 decreases cell proliferation of EWS894 cells (Fig 3.1). To explore whether this effect could be cell-type specific, I asked whether other cell lines of the same cancer type were similarly affected. I treated two additional Ewing sarcoma cell lines, EWS502 and A673, with various concentrations of UNC0621, ranging from 10 μM to 0.15625 μM. I then assayed cell viability 72 hours after treatment using a WST-1 colorimetric assay. As in EWS894 cells, treatment with UNC0621 resulted in a dose-dependent decrease in cell viability in EWS502 and A673 cell lines, demonstrating the sensitivity of multiple Ewing sarcoma cell lines to UNC0621 (Fig 4.1A).

I also wanted to determine how non-Ewing sarcoma cells responded to UNC0621. To determine this, I treated several additional cell lines with the same previously used

concentrations of UNC0621 and assayed cell viability using the same method. Relative to the Ewing sarcoma cells, many cell lines showed decreased sensitivity to UNC0621, including two renal cell carcinoma (UMRC2, 786-O), one primary renal (RPTEC) and a primary endotheilal (HUVEC) cell lines (Fig 4.1B-C). Therefore, Ewing sarcoma cells are exquisitely sensitive to UNC0621 treatment.

Having observed the effect of UNC0621 across many doses, I also wanted to determine the how the compound affects cell viability over time. I treated EWS894 cells in a 96-well plate with 10 μM UNC0621 as assayed viability daily over the course of 6 days. Additionally, I assayed DMSO-treated cells at the same time points as a control. While cells treated with DMSO, showed an expected regular increase in absorbance over time, indicative of increasing cell number, those treated with UNC0621 exhibited a decline in absorbance values over time, indicating a decrease in cell viability (Fig 4.1D).

I then tested whether the effects of UNC0621 persisted after withdrawal of the compound. Following exposure to UNC0621 (or control treatment) for three days, identical numbers of viable cells were placed in growth medium lacking compound and counted daily. UNC0621 exposure delayed the re-initiation of proliferation by approximately two days (Fig 4.1E). These data indicate that a fraction of EWS894 cells remain viable despite UNC0621 treatment and that treatment results in a persistent but reversible effect on proliferation.

Finally, we tested the influence of UNC0621 on anchorage-independent growth, a characteristic feature of cancer cells. Colony formation in soft agar was inhibited at 200 and 400 nM but not at 100 nM. Interestingly, the concentrations associated with absence of colony

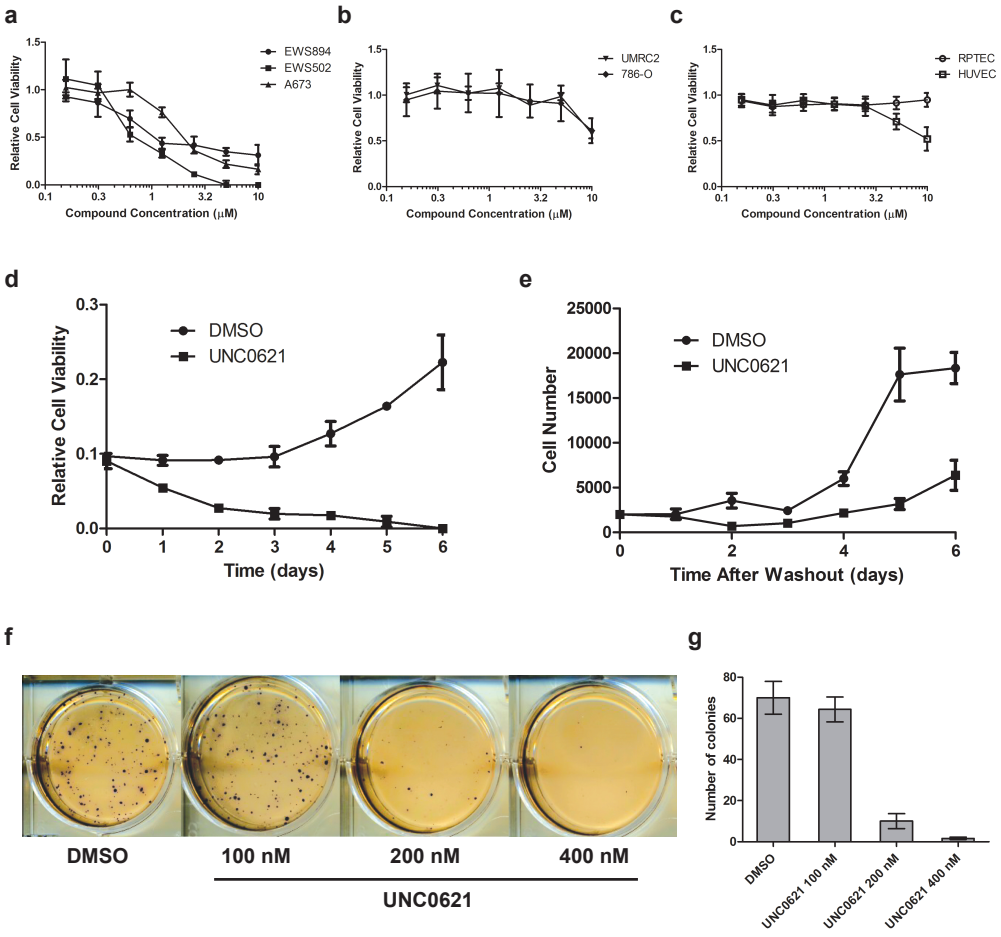

Figure 4.1: UNC0621 affects proliferation, viability and transformation of Ewing sarcoma cells. Dose-dependent effect of UNC0621 on the viability of **(a)** Ewing Sarcoma cell lines, **(b)** renal cell carcinoma cell lines, and **(c)** human primary cells. Cell viability was assayed using WST-1 reagent (Roche) and spectrophotometry. Background absorbance (620 nm) was subtracted from assay absorbance (450 nm) values. Relative cell viability is expressed as $UNC0621^{Abs450\text{-}620}/DMSO^{Abs450\text{-}620}$. Error bars represent standard deviation of three biological replicates. **(d)** Cells were cultured in the presence of 10 μM UNC0621 or 0.1% DMSO for six days, and viability was assessed daily using WST-1 reagent and spectrophotometry. Values are background corrected as above. Error bars represent standard deviation of three biological replicates. **(e)** Cells were grown in the presence of 10 μM UNC0621 or 0.1% DMSO for 3 days. Equal numbers of viable cells were then re-plated in the growth medium in the absence of compound and counted each day for 6 days. Error bars represent standard deviation of triplicate cell counts. **(f)** Effect of UNC0621 on anchorage-independent growth of Ewing Sarcoma cells. EWS894 cells were plated in agar-containing growth media containing UNC0621 or DMSO and incubated for 15 days. Fresh media containing UNC0621 was overlayed and changed every 5 days. Colony formation was assessed on day 15 by MTT assay. **(g)** EWS894 soft agar colony counts. Error bars represent standard deviation of three biological replicates.

formation had minimal effect on viability in short-term culture (Fig 4.1F-G). Taken together, these data demonstrate that UNC0621 has a potent effect on cell viability, proliferation, and transformation in Ewing sarcoma cells.

While metabolic assays such as WST-1 and MTT correlate with the number of live cells, they do not distinguish between a decrease in cell proliferation or an increase in cell death. Due the observation that cells treated with UNC0621 for 3 days continue to proliferate following removal of the compound, I hypothesized that, under the same treatment conditions, UNC0621 does not induce apoptosis. To test this, I measured the apoptotic population of UNC0621-treated EWS894 cells by annexin V staining. Annexin V binds to exposed phosphatidylserine following the inversion of the cell membrane during the early stages of apoptosis. Following staining, I analyzed treated cells by flow cytometry to detect the apoptotic, annexin V cell population. I observed robust annexin V signal in cells that had been treated with staruosporine treatment as a positive control. Interestingly, I observed that after 72 hours of treatment with 10 μM UNC0621, there was no significant difference in the apoptotic population when compared to cells treated DMSO (Fig 4.2). It should be noted that under these treatment conditions, UNC0621 causes a decrease in cell viability as previously measured by WST-1. Therefore, these data suggest that UNC0621 does not affect cell viability through induction of apoptosis.

4.3: UNC0621 inhibits cell cycle progression of Ewing sarcoma cells

As UNC0621 apoptosis did not seem to decrease cell viability through induction of apoptosis, I explored cell cycle arrest as a possible mechanism. If UNC0621 does in fact halt cell cycle progression, then one would expect to observe a lack of cell divisions over time. To directly measure cell division in the presence or absence of UNC0621, I utilized

carboxyfluorescein succinimidyl ester (CFSE) cell staining dye. CFSE is a non-toxic fluorescent dye that covalently binds to intracellular lysine residues and is diluted among daughter cells following cell division. As a result, the fluorescent signal in each cell decreases in intensity as a cell population continues to divide.

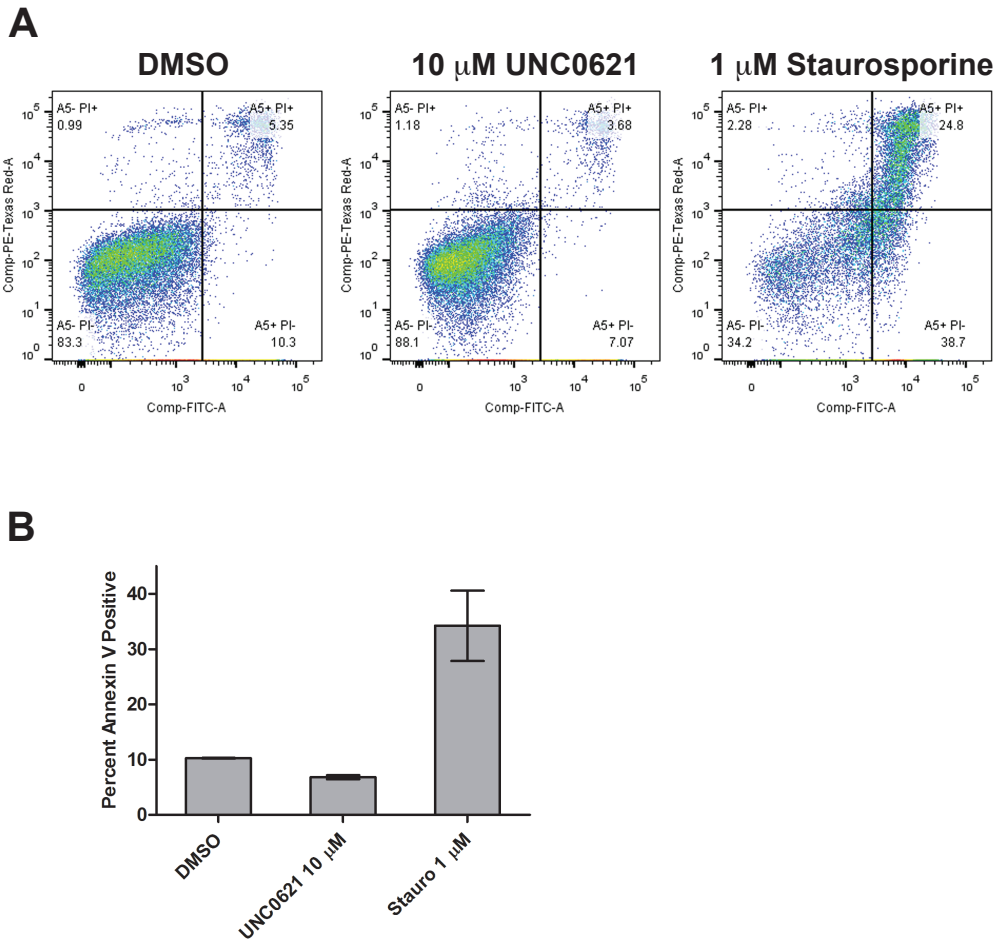

Fig 4.2: UNC0621 does not induce apoptosis in EWS894 cells. A) Cells were stained with annexin V and propidium iodide (PI) after 3 days of treatment, then analyzed by flow cytometry. PI signal is plotted on the y-axis, and annexin V signal on the x-axis. Staurosporine was used as a positive control for the induction of apoptosis. B) Quantification of the apoptotic Annexin V-positive and PI-positive population (upper right quadrant in A).

To determine whether UNC0621 halts cell division, I labeled EWS502 cells with CFSE then divided the labeled cells and treated with UNC0621 or DMSO, with three equal fractions per treatment. I then harvested and fixed a fraction for each treatment condition at 24, 48, or 72 hours following treatment. Additionally, I fixed an equivalent number of untreated cells immediately after staining in order to capture the initial CFSE signal for reference. Following fixation, I quantified CFSE signal in all samples by flow cytometry (Fig 4.3). Cells harvested immediately after staining display high CFSE signal, which is expected as these cells have not divided. Of note, relative to the reference sample, cells treated with DMSO for 24 hours display lower average CFSE signal, indicating progression of cell proliferation. 48 hr DMSO-treated cells exhibit a further decrease in fluorescence, and even lower at 72 hr. These data show that CFSE-labeled cells continue to proliferate in the presence of DMSO as expected. Notably, there is a wide distribution of signal within a single sample, indicating variation in staining likely due to heterogeneity in cell size within the population. In addition, while fluorescence intensity decreases overtime, it does not decrease exactly by half relative to the subsequent time point. This is likely also due to heterogeneity in proliferation within the cell population and imprecise doubling after each 24 hr period.

Upon observing the expected pattern of division among EWS502 cells treated with DMSO, I then compared CFSE-labeled cells treated with UNC0621 (Fig 4.3). 24 hr treatment with UNC0621 results in decreased fluorescence relative to the reference sample, suggesting active proliferation comparable to 24 hr DMSO-treated cells. Interestingly, fluorescence is further diluted in 48 hr UNC0621-treated cells, but this decrease is attenuated in comparison to the corresponding DMSO treatments.

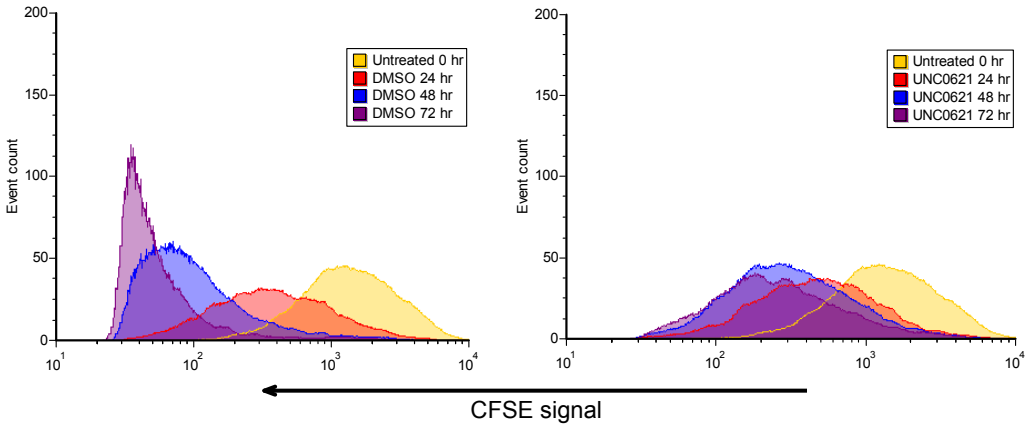

Fig 4.3: UNC0621 inhibits cell division of Ewing sarcoma cells. EWS502 cells were stained with CFSE dye and treated with DMSO (left) or 5 uM UNC0621 (right) for 1, 2 or 3 days. Cells were harvested, fixed, and analyzed by flow cytometry. Both treatment conditions were compared to an untreated stained control (yellow).

Moreover, there is no change in CFSE signal between 48 and 72 hr UNC0621-treated cells. These data suggest that while cells are initially able to divide in the presence of UNC0621, proliferation ultimately slows after two days.

4.4: UNC0621 induces a G0/G1 cell cycle arrest in Ewing sarcoma cells

With quantitative evidence that UNC0621 disrupts cell proliferation, I then sought to determine whether this was due to a cell cycle arrest. To observe the different phases of the cell cycle, I utilized cell staining with propidium iodide followed by flow cytometric analysis. Propidium iodide (PI) is a fluorescent compound that intercalates with DNA, allowing for detection of total DNA content by flow cytometry. Cells in a particular stage of the cell cycle can be identified based on the relative DNA content in that stage. A peak of lower PI signal

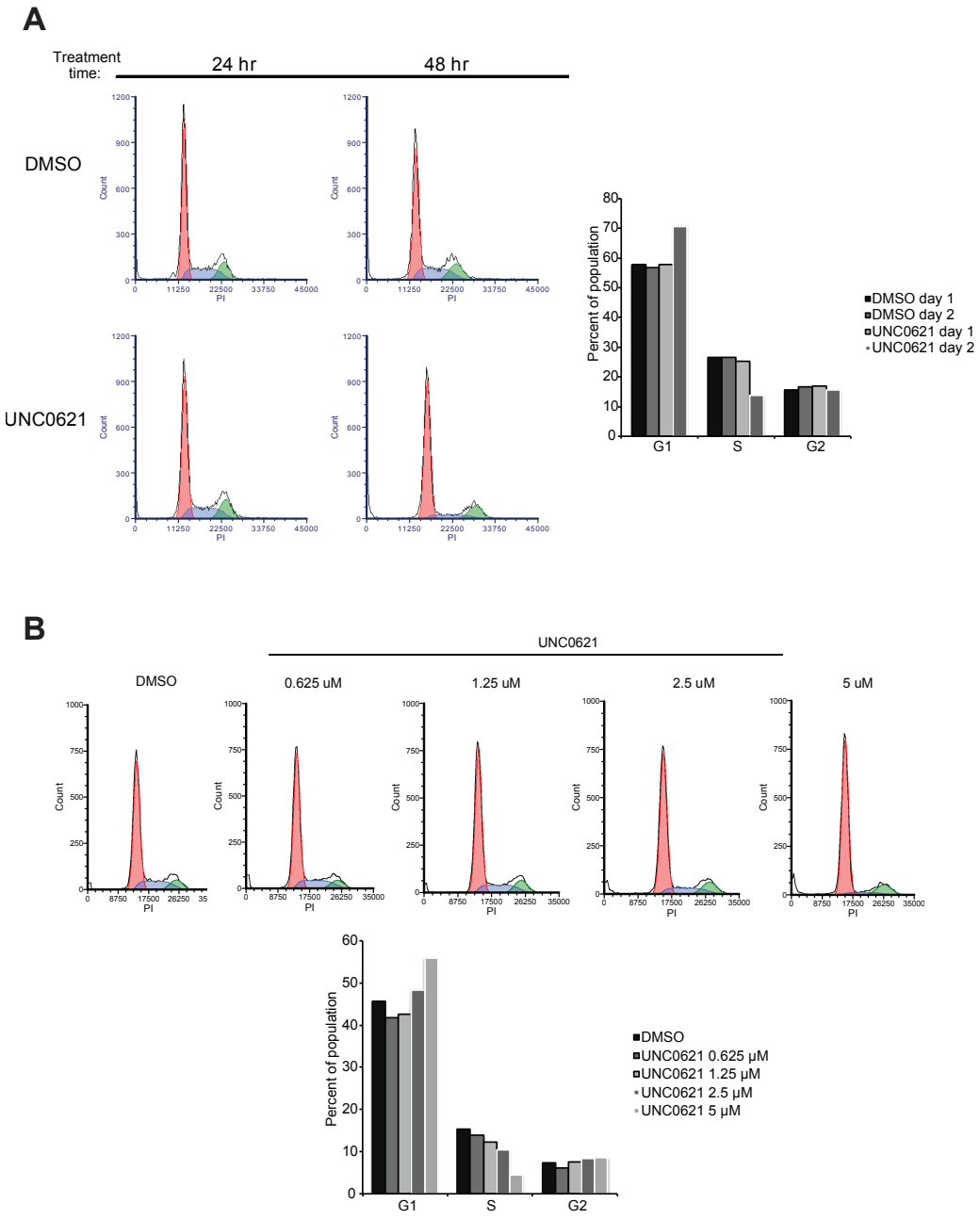

Fig 4.4: UNC0621 causes Ewing sarcoma cells to arrest in G0/G1 of the cell cycle. A) EWS502 cells were treated with 5 uM UNC0621 or DMSO for the indicated periods, then stained with propdium iodide. PI signal was measured by flow cytometry. B) EWS502 cells were treated as indicated for 72 hours, followed by PI staining. All histograms display PI signal on the x-axis and event counts on the y-axis. Graphs represent proportions of population in each stage of the cell cycle estimated for both experiments.

represents the 2N DNA content population is indicative the cells that were G0/G1 phase of the cell cycle at the time of fixation. Cells in G2/M have a DNA content of 4N and appear as a peak with double the PI signal of the 2N peak. S-phase cells have an intermediate DNA content and therefore appear as a continuous population between the 2N and 4N peaks.

To interrogate the effect of UNC0621 on cell cycle progression, I treated EWS502 cells with 5 μM UNC0621 or DMSO for 24 or 48 hours, then stained cells with propidium iodide and analyzed by flow cytometry. In a typical asynchronus cell cycle profile, the 2N peak is generally the highest, indicating that most of the cells are in G0/G1. This is observed in cells treated with DMSO for 24 hours, which displays a tall G0/G1 peak and a shorter G2/M peak separated by an intermediate S-phase population. A similar cell cycle profile is observed in for the 48 hr DMSO-treated sample, showing that cells are dividing similarly at both time points. For EWS502 cells treated with UNC0621 for 24 hr, the cell cycle profile was similar to the corresponding DMSO-treated sample, with the similar proportions in each phase of the cell cycle. However, after 48 hours of UNC0621 treatment, I observed a marked decrease in the S-phase population relative to cells treated with DMSO. This corresponded to an increase in the G0/G1 population, indicating that after 48 hr incubation with UNC0621, cells were accumulating in G1 and unable to progress through S-phase.

To confirm the effect of UNC0621 on cell cycle progression, I sought to test the effect of dose on the cell cycle profile. I treated EWS502 cells with 5, 2.5, 1.25, or 0.625 μM of UNC0621 for 72 hours, then stained with PI and performed cell cycle analysis by flow cytometry. DMSO alone was used as a control. I observed that UNC0621 caused a dose-dependent decrease in the S-phase population, with 5 μM-treated cells having very few cells in

S-phase and the most cells in G0/G1. This further supports that UNC0621 induces a G0/G1 cell cycle arrest in Ewing sarcoma cells.

Although UNC0621 appeared to arrest cell cycle progression as measured by PI staining, the S-phase population is in fact approximated by DNA content. Therefore, I wanted to quantitatively measure the percentage of cells in S-phase using bromodeoxyuridine (BrdU) incorporation. BrdU is a thymidine analog that is incorporated into replicating DNA, and can be detected using antibodies against BrdU, allowing for determination of cells in S-phase at the time of staining. BrdU staining can be combined with a stain for total DNA, in this case 7-AAD. Similar to PI, 7-AAD is a fluorescent intercalating agent, and as such is used to discern different phases of the cell cycle by DNA content. In a dividing cell population, S-phase cells with intermediate 7-AAD signal display an increase in BrdU signal after the 2N population, then signal decreases approaching the 4N population.

I hypothesized that cells treated with UNC0621 for longer periods of time (48 or 72 hr) would have a decreased BrdU-positive population than control cells. To test this, I treated EWS502 cells with DMSO or 5 uM UNC0621 for 24, 48, or 72 hours, followed by a pulse with BrdU to label cells undergoing DNA replication. I also stained cells with 7-AAD to measure total DNA, then analyzed by flow cytometry. In 24 hr DMSO-treated cells, I observed the 2N (G0/G1) and 4N (G2/M) populations by low and high 7-AAD signal. These populations were also negative for BrdU incorporation. In between these populations I observed a BrdU-positive S-phase population, representing about 36% of captured events. 48 and 72 hr DMSO-treated samples show a similar pattern of BrdU incorporation, indicating that all DMSO-treated samples, regardless of treatment time, had comparable percentages of actively replicating cells at the time of staining.

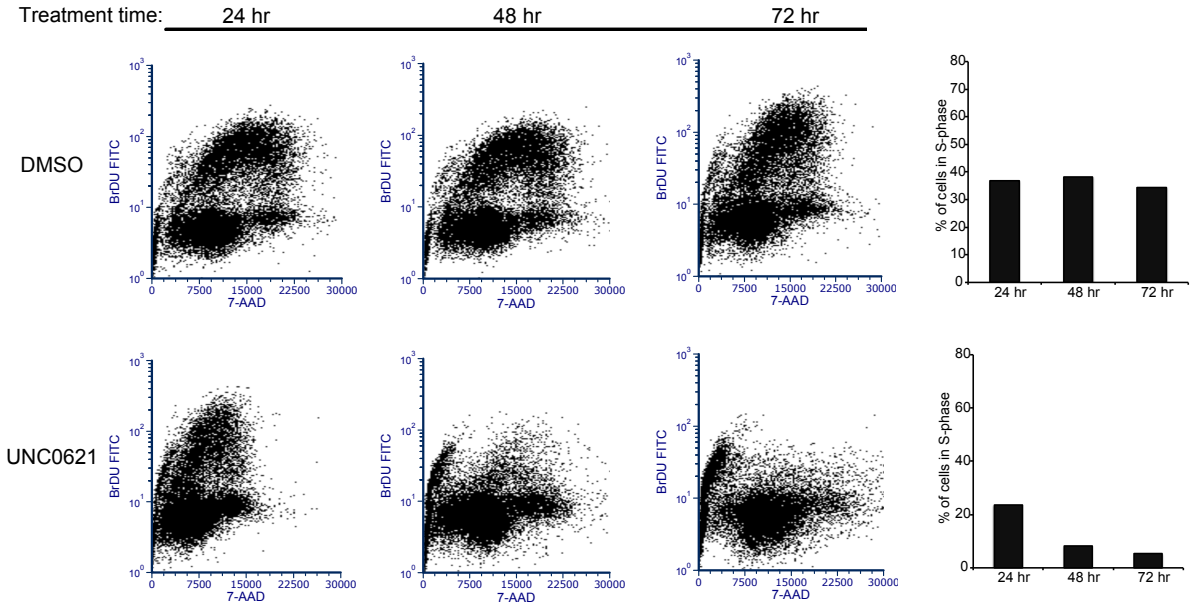

Fig 4.5: UNC0621 decreases the S-phase population of Ewing sarcoma cells. EWS502 cells were treated with DMSO or 5 uM for the indicated period of time, then pulsed with BrdU for 1 hour. Cells were then harvested and fixed, and analyzed by flow cytometry. Representative experiment is shown. FITC-BrdU signal is on the y-axis, and 7-AAD signal is on the x-axis. Graphs depict quantification of BrdU-positive population.

Comparing the cells treated with UNC0621, the 24 hr sample exhibited a slightly lower percentage of BrdU-positive cells, about 24% of the population relative to 35% seen in 24 hr DMSO-treated cells. Strikingly, after 48 hours of UNC0621 treatment, the BrdU-positive population decreased to about 8% of the total population, and further to 4% after 72 hours of treatment. These data quantitatively demonstrate that UNC0621 treatment decreases active replication of Ewing sarcoma cells, and corroborates cell cycle profile experiments showing an arrest of cells in G0/G1.

4.5: Discussion

My use of cell biological approaches has revealed that UNC0621 in an inducer of cell cycle arrest in Ewing sarcoma, rather than apoptosis. However, while cell lines that possess relative resistance to UNC0621 show this effect is not general, it is also not selective for Ewing

sarcoma. Many other cell lines, including Jurkat, MSC, and SCCOHT also displayed sensitivity to UNC0621 comparable to that of Ewing sarcoma cells. There are likely underlying biological differences or dependencies that dictate sensitivity to UNC0621, although this is not readily apparent. One current goal is to analyze alterations caused by UNC0621 to determine changes in genes or pathways that may mediate a cell cycle arrest phenotype. Moreover, changes detected by RNA-seq that are shared between sensitive cell lines may point to a biological mechanism for the phenotypes mediated by UNC0621.

4.6: Methods

Cell culture

EWS894 and EWS502 cells (42) were cultured in RPMI-1640 supplemented with 15% FBS. A673 cells were cultured in RPMI-1640 with 10% FBS. UMRC2 and 786-O cells were cultured in DMEM with sodium pyruvate, L-glutamine and 4.5 g/L glucose, supplemented with 10% FBS. RPTEC cells were cultured using the REGM™ BulletKit™ (Lonza). HUVEC cells were cultured in the EGM™-2 BulletKit™ (Lonza) supplemented with 10% FBS and maintained at standard growth conditions of 37 °C and 5% CO2.

Viability Assays

Cell viability was assessed by WST-1 (Roche Applied Sciences) according to manufacturer's recommendations. Absorbance was quantified at 450 nm and background scatter measured at 620 nm, with the latter value subtracted from 450 nm value to obtain the final absorbance. The background absorbance (media only) was subtracted from the mean of the triplicates for each condition. Relative absorbance is expressed as a ratio of UNC0621-treated

over DMSO-treated. Error bars indicate standard deviation between three technical replicates. Cells counts were performed using a hemocytometer.

Soft agar colony growth

Cells were suspended in 0.5% low melting point agarose, 1X RPMI, 15% fetal bovine serum at a density of 4500 cells per well and layered over one mL of base agar (0.6% agarose, 1X RPMI, 15% fetal bovine serum) in a 6-well dish. UNC0621 or DMSO was diluted in top agar layer to desired final concentration. Plates were overlayed with additional RPMI containing compound on day 5 and day 11. Plates were stained with MTT (0.5 mg/ml) on day 15 to visualize cell colonies.

Apoptosis

Cells were prepared and stained using BD Pharmingen™ FITC Annexin V Apoptosis Detection Kit and protocol (cat. No. 556547). Flow cytometry was performed immediately after staining (LSR II).

Cell cycle analysis

Treated cells were washed with PBS and fixed with 70% ice cold ethanol, then stained with PI. Flow cytometry was performed immediately after staining, collecting 10,000 total events at 100-200 events per second (CyAN, Beckman Coulter).

Chapter 5: Conclusions and Discussion

In this study, we sought to identify and characterize small molecules that can reverse the chromatin signature mediated by the EWSR1-FLI1 oncogenic driver found in Ewing sarcoma, as discussed in Chapter 1. Using a novel chromatin-based screening approach, we discovered small molecule regulators of aberrant chromatin accessibility in Ewing sarcoma. While we focused our initial efforts on Ewing sarcoma, this approach could conceivably be applied to any cancer with a known chromatin signature.

Our screen identified histone deacetylase inhibitors (HDACi) as the primary compound class causing reversal of the oncogenic chromatin signature. This phenotype appears to be caused by the ability of HDACi to decrease transcription of the *EWSR1-FLI1* fusion gene. Upon subsequent cursory examination of endogenous transcript levels of parental EWSR1 gene, we observed that HDACi treatment also decreased *EWSR1* transcript levels. This mechanism of action points to a potential role of HDAC proteins in regulating transcript levels of *EWSR1-FLI1* via interaction with the *EWSR1* promoter. To better understand this process, more work needs to be done in determining the regulatory factors that occupy the *EWSR1* promoter.

Additionally, we have identified UNC0621 as an inhibitor of chromatin accessibility and cell cycle progression in Ewing sarcoma. A looming concern is whether there is a link between the effect of UNC0621 on chromatin and on cell biology. UNC0621 seems to have an affinity for histone proteins, which are generally abundant across cell types. However, UNC0621 has a selective affect on cell proliferation. This discrepancy has several possible explanations. For instance, it is possible that UNC0621 derivatives bind ubiquitously to histones in vitro, but in

reality UNC0621 binds a subset of histones in cells. These could be marked by a post-translational modification or by the presence of another regulatory factor that interacts with the compound. To determine this, we aim to perform in vivo Chem-seq to capture genome-wide interactions of the compound in vivo. Succeeding in this effort will provide insight into regions of the genome that may be selectively targeted by the UNC0621.

The biological determinants for sensitivity of a particular cell type to UNC0621 are still not understood. We have already performed RNA-seq in EWS894 cells and observed widespread changes in gene expression following treatment with UNC0621. We are currently performing RNA-seq in both sensitive and resistant cell lines following UNC0621 treatment to determine whether there are gene expression changes shared between cell lines that could begin to elucidate the mechanism of cell cycle arrest by UNC0621.

It is also possible that UNC0621 exhibits widespread binding across the genome, but only displays activity on certain regions of chromatin. To determine how UNC0621 affects chromatin accessibility genome-wide, we aim to perform FAIRE-seq in cells following treatment with UNC0621. Our attempts have been wrought with technical difficulties over the years, but we are now seeing signs of success and will soon be able to interrogate how UNC0621 regulates the epigenome.

Yet another possible reason for our observations is that UNC0621 binds to a nucleosome-associated protein target other than histones. Histones might appear frequently in our in vitro pull-downs due to their abundance, but it is possible they are not the primary biological target. Ongoing proteomic studies will provide candidates for biochemical targets of UNC0621.

Ultimately, our understanding of the function of chromatin-targeted small molecules would benefit greatest from comprehensive genomic characterization. Comparison of compound-

induced chromatin and gene expression signatures across cell types can shed light on a compound's mechanism of action and potential therapeutic utility. While we have begun this process for UNC0621, there are still many questions to be answered. Ideally UNC0621 can become a useful tool compound to study epigenetic processes important for certain cancers. Similar approaches for other chromatin-targeted small molecules will contribute to the study of cancers with epigenetic aberrations, both from a perspective of understanding regulatory mechanisms as well as creating potential for targeted therapies.

REFERENCES

1. Qiu J. Epigenetics: unfinished symphony. Nature. 2006;441(May):143–5.

2. Zhou VW, Goren A, Bernstein BE. Charting histone modifications and the functional organization of mammalian genomes. Nat Rev Genet [Internet]. Nature Publishing Group; 2011;12(1):7–18. Available from: http://www.ncbi.nlm.nih.gov/pubmed/21116306

3. Tsompana M, Buck MJ. Chromatin accessibility: a window into the genome. Epigenetics Chromatin [Internet]. 2014;7(1):33. Available from: http://www.epigeneticsandchromatin.com/content/7/1/33

4. Bitler BG, Aird KM, Garipov A, Li H, Amatangelo M, Kossenkov A V, et al. Synthetic lethality by targeting EZH2 methyltransferase activity in ARID1A-mutated cancers. Nat Med [Internet]. Nature Publishing Group; 2015 Feb 16 [cited 2015 Feb 17];(August 2014):1–10. Available from: http://www.ncbi.nlm.nih.gov/pubmed/25686104

5. Paulsen M, Ferguson-smith AC. DNA methylation in genomic imprinting , development , and disease. 2001;97–110.

6. Strahl BD, Allis CD. The language of covalent histone modifications. Nature [Internet]. 2000;403(6765):41–5. Available from: http://www.nature.com/doifinder/10.1038/47412

7. Wilson BG, Roberts CWM. SWI/SNF nucleosome remodellers and cancer. Nat Rev Cancer [Internet]. 2011 Jul [cited 2014 Mar 19];11(7):481–92. Available from: http://www.ncbi.nlm.nih.gov/pubmed/21654818

8. Maier VK, Becker PB. Chromatin Remodeling. Morse RH, editor. Totowa, NJ: Humana Press; 2012 [cited 2014 Mar 19];833:255–70. Available from: http://link.springer.com/10.1007/978-1-61779-477-3

9. Gaffney DJ, McVicker G, Pai A a, Fondufe-Mittendorf YN, Lewellen N, Michelini K, et al. Controls of nucleosome positioning in the human genome. PLoS Genet [Internet]. 2012 Jan [cited 2014 Jul 11];8(11):e1003036. Available from: http://www.pubmedcentral.nih.gov/articlerender.fcgi?artid=3499251&tool=pmcentrez&rendertype=abstract

10. Park PJ. ChIP–seq: advantages and challenges of a maturing technology. Nat Rev Genet [Internet]. 2009;10(10):669–80. Available from: http://www.nature.com/doifinder/10.1038/nrg2641

11. Romanoski CE, Glass CK, Stunnenberg HG, Wilson L, Almouzni G. Epigenomics: Roadmap for regulation. Nature [Internet]. 2015;518(7539):314–6. Available from: http://www.nature.com/doifinder/10.1038/518314a

12. Bernstein BE, Birney E, Dunham I, Green ED, Gunter C, Snyder M. An integrated encyclopedia of DNA elements in the human genome. Nature [Internet]. 2012 Sep 6 [cited 2014 Jul 9];489(7414):57–74. Available from: http://www.pubmedcentral.nih.gov/articlerender.fcgi?artid=3439153&tool=pmcentrez&rendertype=abstract

13. Stratton MR, Campbell PJ, Futreal PA. The Cancer Genome Atlas. Nature [Internet]. 2009;458:719–24. Available from: http://www.pubmedcentral.nih.gov/articlerender.fcgi?artid=2821689&tool=pmcentrez&rendertype=abstract%5Cnhttp://cancergenome.nih.gov/

14. Shen H, Laird PW. Interplay between the cancer genome and epigenome. Vol. 153, Cell. 2013. p. 38–55.

15. Plass C, Pfister SM, Lindroth AM, Bogatyrova O, Claus R, Lichter P. Mutations in regulators of the epigenome and their connections to global chromatin patterns in cancer. Nat Rev Genet [Internet]. 2013;14(11):765–80. Available from: http://www.nature.com/doifinder/10.1038/nrg3554

16. Mehdi A, Riazalhosseini Y. Epigenome Aberrations: Emerging Driving Factors of the Clear Cell Renal Cell Carcinoma. Int J Mol Sci [Internet]. 2017;18(8):1774. Available from: http://www.ncbi.nlm.nih.gov/pubmed/28812986%0Ahttp://www.mdpi.com/1422-0067/18/8/1774

17. Kuwahara Y, Wei D, Durand J, Weissman BE. SNF5 reexpression in malignant rhabdoid tumors regulates transcription of target genes by recruitment of SWI/SNF complexes and RNAPII to the transcription start site of their promoters. Mol Cancer Res [Internet]. 2013 Mar [cited 2014 Mar 19];11(3):251–60. Available from: http://www.ncbi.nlm.nih.gov/pubmed/23364536

18. Wee S, Dhanak D, Li H, Armstrong S a, Copeland R a, Sims R, et al. Targeting epigenetic regulators for cancer therapy. Ann N Y Acad Sci [Internet]. 2014 Feb [cited 2014 May 5];1309:30–6. Available from: http://www.ncbi.nlm.nih.gov/pubmed/24571255

19. Hamm CA, Costa FF. Epigenomes as therapeutic targets. Pharmacol Ther [Internet]. Elsevier Inc.; 2015;151:72–86. Available from: http://dx.doi.org/10.1016/j.pharmthera.2015.03.003

20. Dhanak D, Jackson P. Development and classes of epigenetic drugs for cancer. Biochem Biophys Res Commun [Internet]. Elsevier Inc.; 2014 Jul 10 [cited 2014 Aug 17]; Available from: http://www.ncbi.nlm.nih.gov/pubmed/25016182

21. Christman JK, Mendelsohn N, Herzog D. Effect of 5-Azacytidine on Differentiation and DNA Methylation in Human Promyelocyte Leukemia Cells (HL-60). 1983;763–9.

22. Raj K, Mufti GJ. Azacytidine (Vidaza®) in the treatment of myelodysplastic syndromes. Vol. 2, Therapeutics and Clinical Risk Management. 2006. p. 377–88.

23. Dokmanovic M, Clarke C, Marks P a. Histone deacetylase inhibitors: overview and perspectives. Mol Cancer Res [Internet]. 2007 Oct [cited 2014 Mar 19];5(10):981–9. Available from: http://www.ncbi.nlm.nih.gov/pubmed/17951399

24. Laubach JP, Moreau P, San-Miguel JF, Richardson PG. Panobinostat for the Treatment of Multiple Myeloma. Clin Cancer Res [Internet]. 2015;21(21):4767–73. Available from: http://www.ncbi.nlm.nih.gov/pubmed/26362997

25. Pachaiyappan B, Woster PM. Design of small molecule epigenetic modulators. Bioorg Med Chem Lett [Internet]. Elsevier Ltd; 2014 Jan 1 [cited 2014 Aug 5];24(1):21–32. Available from: http://www.ncbi.nlm.nih.gov/pubmed/24300735

26. Vedadi M, Barsyte-lovejoy D, Liu F, Rival-gervier S, Allali-hassani A, Labrie V, et al. A chemical probe selectively inhibits G9a and GLP methyltransferase activity in cells. 2011;7(august).

27. He Y, Korboukh I, Jin J, Huang J. Targeting protein lysine methylation and demethylation in cancers Proteins that are Subject to Lysine Methylation Potential Biological Functions of PKMTs in Cancers. 2012;44(1):70–9.

28. Bose P, Dai Y, Grant S. Histone deacetylase inhibitor (HDACI) mechanisms of action: Emerging insights. Pharmacol Ther [Internet]. Elsevier Inc.; 2014 Apr 23 [cited 2014 Apr 30]; Available from: http://www.ncbi.nlm.nih.gov/pubmed/24769080

29. McCabe MT, Creasy CL. EZH2 as a potential target in cancer therapy. Epigenomics [Internet]. 2014 Jun;6(3):341–51. Available from: http://www.ncbi.nlm.nih.gov/pubmed/25111487

30. McCabe MT, Ott HM, Ganji G, Korenchuk S, Thompson C, Van Aller GS, et al. EZH2 inhibition as a therapeutic strategy for lymphoma with EZH2-activating mutations. Nature [Internet]. Nature Publishing Group; 2012 Dec 6 [cited 2014 Jul 11];492(7427):108–12. Available from: http://www.ncbi.nlm.nih.gov/pubmed/23051747

31. Allis CD, Jenuwein T. The molecular hallmarks of epigenetic control. Nat Rev Genet [Internet]. Nature Publishing Group; 2016;17(8):487–500. Available from: http://www.nature.com/doifinder/10.1038/nrg.2016.59

32. Filippakopoulos P, Qi J, Picaud S, Shen Y, Smith WB, Fedorov O, et al. Selective inhibition of BET bromodomains. Nature [Internet]. Nature Publishing Group; 2010 Dec 23 [cited 2014 Jul 17];468(7327):1067–73. Available from: http://www.pubmedcentral.nih.gov/articlerender.fcgi?artid=3010259&tool=pmcentrez&rendertype=abstract

33. Shin DG, Bayarsaihan D. A novel epi-drug therapy based on the suppression of BET family epigenetic readers. Yale J Biol Med. 2017;90(1):63–71.

34. Mertz J a, Conery AR, Bryant BM, Sandy P, Balasubramanian S, Mele D a, et al. Targeting MYC dependence in cancer by inhibiting BET bromodomains. Proc Natl Acad Sci U S A [Internet]. 2011 Oct 4 [cited 2014 Jul 15];108(40):16669–74. Available from: http://www.pubmedcentral.nih.gov/articlerender.fcgi?artid=3189078&tool=pmcentrez&rendertype=abstract

35. Asangani I a, Dommeti VL, Wang X, Malik R, Cieslik M, Yang R, et al. Therapeutic targeting of BET bromodomain proteins in castration-resistant prostate cancer. Nature [Internet]. 2014 Jun 12 [cited 2014 Jul 10];510(7504):278–82. Available from: http://www.ncbi.nlm.nih.gov/pubmed/24759320

36. Kim SK, Park YK. Ewing sarcoma: A chronicle of molecular pathogenesis. Hum Pathol. 2016;55:91–100.

37. Delattre O, Zucman J, Melot T, Garau XS, Zucker JM, Lenoir GM, et al. The Ewing family of tumors--a subgroup of small-round-cell tumors defined by specific chimeric transcripts. N Engl J Med [Internet]. 1994;331(5):294–9. Available from: http://www.ncbi.nlm.nih.gov/pubmed/8022439

38. Hromas R, Denny CT, May WA, Lessnick SL, Braun BS, Klemsz M, et al. The Ewing ' s Sarcoma EWS / FLI-1 Fusion Gene Encodes a More Potent Transcriptional Activator and Is a More Powerful Transforming Gene than FLI-i. 1993;

39. Bailly R, Bosselut R, Zucman J, Delattre O, Roussel M, Thomas G, et al. DNA-Binding and Transcriptional Activation Properties of the EWS-FLI-1 Fusion Protein Resulting from the t (11 ; 22) Translocation in Ewing Sarcoma FLI-1 BsaHI-to-BamHI BglII-bor-HindlIl HindIII Ets-l (C) EcoRI Ets-l (C) EcoRI polyII . Gal4-FLI-1 (. 1994;14(5):3230–41.

40. Kinsey M, Smith R, Iyer AK, McCabe ERB, Lessnick SL. EWS/FLI and its downstream target NR0B1 interact directly to modulate transcription and oncogenesis in Ewing's sarcoma. Cancer Res [Internet]. 2009 Dec 1 [cited 2014 Mar 19];69(23):9047–55. Available from: http://www.pubmedcentral.nih.gov/articlerender.fcgi?artid=2789197&tool=pmcentrez&rendertype=abstract

41. Erkizan H V, Uversky VN, Toretsky J a. Oncogenic partnerships: EWS-FLI1 protein interactions initiate key pathways of Ewing's sarcoma. Clin Cancer Res [Internet]. 2010 Aug 15 [cited 2014 Mar 19];16(16):4077–83. Available from: http://www.pubmedcentral.nih.gov/articlerender.fcgi?artid=3682924&tool=pmcentrez&rendertype=abstract

42. Patel M, Simon JM, Iglesia MD, Wu SB, McFadden AW, Lieb JD, et al. Tumor-specific retargeting of an oncogenic transcription factor chimera results in dysregulation of

chromatin and transcription. Genome Res [Internet]. 2012 Feb [cited 2014 Jul 14];22(2):259–70. Available from: http://www.pubmedcentral.nih.gov/articlerender.fcgi?artid=3266033&tool=pmcentrez&rendertype=abstract

43. Li Y, Luo H, Liu T, Zacksenhaus E, Ben-David Y. The ets transcription factor Fli-1 in development, cancer and disease. Oncogene [Internet]. 2014;(February):1–10. Available from: http://www.ncbi.nlm.nih.gov/pubmed/24909161

44. Cantile M, Marra L, Franco R, Ascierto P, Liguori G, De Chiara A, et al. Molecular detection and targeting of EWSR1 fusion transcripts in soft tissue tumors. Med Oncol. 2013;30(1).

45. Yu H, Ge Y, Guo L, Huang L, Yu H, Ge Y, et al. Potential approaches to the treatment of Ewing's sarcoma. Oncotarget [Internet]. 2015;5(0):5523–39. Available from: http://www.oncotarget.com/abstract/12566

46. Waldmann T, Schneider R. Targeting histone modifications - epigenetics in cancer. Curr Opin Cell Biol. 2013;25(2):184–9.

47. Kaniskan HÜ, Konze KD, Jin J. Selective inhibitors of protein methyltransferases. J Med Chem. 2015;58(4):1596–629.

48. Daigle SR, Olhava EJ, Therkelsen CA, Basavapathruni A, Jin L, Boriack-Sjodin PA, et al. Potent inhibition of DOT1L as treatment of MLL-fusion leukemia. Blood. 2013;122(6):1017–25.

49. Qi W, Chan H, Teng L, Li L, Chuai S, Zhang R, et al. Selective inhibition of Ezh2 by a small molecule inhibitor blocks tumor cells proliferation. Proc Natl Acad Sci. 2012;109:21360–5.

50. Konze KD, Ma A, Li F, Barsyte-Lovejoy D, Parton T, MacNevin CJ, et al. An orally bioavailable chemical probe of the lysine methyltransferases EZH2 and EZH1. ACS Chem Biol. 2013;8(6):1324–34.

51. Vedadi M, Barsyte-Lovejoy D, Liu F, Rival-Gervier S, Allali-Hassani A, Labrie V, et al. A chemical probe selectively inhibits G9a and GLP methyltransferase activity in cells. Nat Chem Biol [Internet]. 2011;7(8):566–74. Available from: http://www.nature.com/doifinder/10.1038/nchembio.599

52. Liu F, Barsyte-Lovejoy D, Li F, Xiong Y, Korboukh V, Huang XP, et al. Discovery of an in vivo chemical probe of the lysine methyltransferases G9a and GLP. J Med Chem. 2013;56(21):8931–42.

53. James LI, Barsyte-Lovejoy D, Zhong N, Krichevsky L, Korboukh VK, Herold JM, et al. Discovery of a chemical probe for the L3MBTL3 methyllysine reader domain. Nat Chem

Biol [Internet]. 2013;9(3):184–91. Available from: http://www.nature.com/doifinder/10.1038/nchembio.1157

54. French C a, Ramirez CL, Kolmakova J, Hickman TT, Cameron MJ, Thyne ME, et al. BRD-NUT oncoproteins: a family of closely related nuclear proteins that block epithelial differentiation and maintain the growth of carcinoma cells. Oncogene [Internet]. 2008 Apr 3 [cited 2014 Aug 26];27(15):2237–42. Available from: http://www.ncbi.nlm.nih.gov/pubmed/17934517

55. Delattre O, Zucman J, Plougastel B, Desmaze C, Melot T, Peter M, et al. Gene fusion with an ETS DNA-binding domain caused by chromosome translocation in human tumours. Nature [Internet]. 1992;359(6391):162–5. Available from: http://www.nature.com/doifinder/10.1038/359162a0%5Cnhttp://www.ncbi.nlm.nih.gov/pubmed/1522903

56. Gangwal K, Close D, Enriquez C a., Hill CP, Lessnick SL. Emergent Properties of EWS/FLI Regulation via GGAA Microsatellites in Ewing's Sarcoma. Genes Cancer [Internet]. 2010 Feb 1 [cited 2014 Mar 19];1(2):177–87. Available from: http://www.pubmedcentral.nih.gov/articlerender.fcgi?artid=2935179&tool=pmcentrez&rendertype=abstract

57. Simon JM, Giresi PG, Davis IJ, Lieb JD. Using formaldehyde-assisted isolation of regulatory elements (FAIRE) to isolate active regulatory DNA. Nat Protoc [Internet]. Nature Publishing Group; 2012 Feb [cited 2014 Mar 25];7(2):256–67. Available from: http://www.pubmedcentral.nih.gov/articlerender.fcgi?artid=3784247&tool=pmcentrez&rendertype=abstract

58. Song L, Zhang Z, Grasfeder LL, Boyle AP, Giresi PG, Lee BK, et al. Open chromatin defined by DNaseI and FAIRE identifies regulatory elements that shape cell-type identity. Genome Res. 2011;21(10):1757–67.

59. McLean CY, Bristor D, Hiller M, Clarke SL, Schaar BT, Lowe CB, et al. GREAT improves functional interpretation of cis-regulatory regions. Nat Biotechnol [Internet]. 2010;28(5):495–501. Available from: http://www.nature.com/doifinder/10.1038/nbt.1630

60. De Val S, Black BL. Transcriptional Control of Endothelial Cell Development. Vol. 16, Developmental Cell. 2009. p. 180–95.

61. Meadows SM, Myers CT, Krieg PA. Regulation of endothelial cell development by ETS transcription factors. Semin Cell Dev Biol [Internet]. 2011;22(9):976–84. Available from: http://www.ncbi.nlm.nih.gov/pubmed/21945894%5Cnhttp://www.pubmedcentral.nih.gov/articlerender.fcgi?artid=PMC3263765

62. Malo N, Hanley JA, Cerquozzi S, Pelletier J, Nadon R. Statistical practice in high-throughput screening data analysis. Nat Biotechnol [Internet]. 2006;24(2):167–75. Available from: http://www.nature.com/doifinder/10.1038/nbt1186

63. Caraus I, Alsuwailem AA, Nadon R, Makarenkov V. Detecting and overcoming systematic bias in highthroughput screening technologies: A comprehensive review of practical issues and methodological solutions. Brief Bioinform. 2015;16(6):974–86.

64. Butler K V., Kalin J, Brochier C, Vistoli G, Langley B, Kozikowski AP. Rational design and simple chemistry yield a superior, neuroprotective HDAC6 inhibitor, tubastatin A. J Am Chem Soc. 2010;132(31):10842–6.

65. Balasubramanian S, Ramos J, Luo W, Sirisawad M, Verner E, Buggy JJ. A novel histone deacetylase 8 (HDAC8)-specific inhibitor PCI-34051 induces apoptosis in T-cell lymphomas. Leukemia [Internet]. 2008;22(5):1026–34. Available from: http://www.nature.com/doifinder/10.1038/leu.2008.9

66. Falkenberg KJ, Johnstone RW. Histone deacetylases and their inhibitors in cancer, neurological diseases and immune disorders. Nat Rev Drug Discov [Internet]. 2014;13(9):673–91. Available from: http://www.nature.com/doifinder/10.1038/nrd4360

67. Sankar S, Theisen ER, Bearss J, Mulvihill T, Hoffman LM. Reversible LSD1 inhibition interferes with global EWS / ETS transcriptional activity and impedes Ewing sarcoma tumor growth. 2013;

68. Kovar H. Blocking the road, stopping the engine or killing the driver? Advances in targeting EWS/FLI-1 fusion in Ewing sarcoma as novel therapy. Expert Opin Ther Targets [Internet]. 2014;18(11):1315–28. Available from: http://www.ncbi.nlm.nih.gov/pubmed/25162919%5Cnhttp://www.tandfonline.com/doi/full/10.1517/14728222.2014.947963

69. Boro a, Pretre K, Rechfeld F, Thalhammer V, Oesch S, Wachtel M, et al. Small-molecule screen identifies modulators of EWS/FLI1 target gene expression and cell survival in Ewing's sarcoma. Int J Cancer [Internet]. 2012 Nov 1 [cited 2014 Mar 19];131(9):2153–64. Available from: http://www.ncbi.nlm.nih.gov/pubmed/22323082

70. Owen L a, Kowalewski A a, Lessnick SL. EWS/FLI mediates transcriptional repression via NKX2.2 during oncogenic transformation in Ewing's sarcoma. PLoS One [Internet]. 2008 Jan [cited 2014 Mar 23];3(4):e1965. Available from: http://www.pubmedcentral.nih.gov/articlerender.fcgi?artid=2291578&tool=pmcentrez&rendertype=abstract

71. Simon JM, Hacker KE, Singh D, Brannon a R, Parker JS, Weiser M, et al. Variation in chromatin accessibility in human kidney cancer links H3K36 methyltransferase loss with widespread RNA processing defects. Genome Res [Internet]. 2014 Feb [cited 2014 Jul 16];24(2):241–50. Available from: http://www.ncbi.nlm.nih.gov/pubmed/24158655

72. Sakimura R, Tanaka K, Nakatani F, Matsunobu T, Li X, Hanada M, et al. Antitumor effects of histone deacetylase inhibitor on Ewing's family tumors. Int J Cancer [Internet]. 2005 Sep 20 [cited 2014 Mar 19];116(5):784–92. Available from: http://www.ncbi.nlm.nih.gov/pubmed/15849726

73. Delcuve GP, Khan DH, Davie JR. Targeting class I histone deacetylases in cancer therapy. Expert Opin Ther Targets. 2012;8222(December):1–13.

74. Jeon YJ, Ko SM, Cho JH, Chae J Il, Shim JH. The HDAC inhibitor, panobinostat, induces apoptosis by suppressing the expresssion of specificity protein 1 in oral squamous cell carcinoma. Int J Mol Med. 2013;32(4):860–6.

75. Kim YJ, Greer CB, Cecchini KR, Harris LN, Tuck DP, Kim TH. HDAC inhibitors induce transcriptional repression of high copy number genes in breast cancer through elongation blockade. Oncogene [Internet]. 2013;32(23):2828–35. Available from: http://www.nature.com/doifinder/10.1038/onc.2013.32

76. Livak KJ, Schmittgen TD. Analysis of relative gene expression data using real-time quantitative PCR and the 2(-Delta Delta C(T)) Method. Methods [Internet]. 2001;25(4):402–8. Available from: http://www.ncbi.nlm.nih.gov/pubmed/11846609

77. Anders L, Guenther MG, Qi J, Fan ZP, Marineau JJ, Rahl PB, et al. Genome-wide localization of small molecules. Nat Biotechnol [Internet]. 2014 Jan [cited 2014 Jul 9];32(1):92–6. Available from: http://www.ncbi.nlm.nih.gov/pubmed/24336317

78. Konze KD, Pattenden SG, Liu F, Barsyte-Lovejoy D, Li F, Simon JM, et al. A chemical tool for in vitro and in vivo precipitation of lysine methyltransferase G9a. ChemMedChem [Internet]. 2014 Mar [cited 2014 Oct 12];9(3):549–53. Available from: http://www.ncbi.nlm.nih.gov/pubmed/24443078

79. Park YJ, Dyer PN, Tremethick DJ, Luger K. A new fluorescence resonance energy transfer approach demonstrates that the histone variant H2AZ stabilizes the histone octamer within the nucleosome. J Biol Chem. 2004;279(23):24274–82.

80. Ruthenburg AJ, Li H, Milne TA, Dewell S, McGinty RK, Yuen M, et al. Recognition of a mononucleosomal histone modification pattern by BPTF via multivalent interactions. Cell [Internet]. Elsevier Inc.; 2011;145(5):692–706. Available from: http://dx.doi.org/10.1016/j.cell.2011.03.053